Electronic Supplementary Material (ESI) for Dalton Transactions.

Fluorinated tris(pyridyl)borate ligand support on coinage metals

Mukundam Vanga, Alvaro Muñoz-Castro and H. V. Rasika Dias

Supporting information

General Procedures.

All preparations and manipulations were carried out under an atmosphere of purified nitrogen using standard Schlenk techniques or in a MBraun drybox equipped with a -25 °C refrigerator. Commercially available solvents were purified and dried by standard methods. Glassware was oven dried overnight at 150 °C. NMR spectra were acquired at 25 °C, on a JEOL Eclipse 500 spectrometer (^{1}H, 500 MHz; ^{13}C, 126 MHz; ^{19}F, 471 MHz), and a JEOL Eclipse 300 spectrometer (^{11}B, 96 MHz). ^{19}F NMR values were referenced to external $CFCl_3$. ^{1}H and ^{13}C{^{1}H} NMR spectra were referenced internally to solvent signals ($CDCl_3$: 7.26 ppm for ^{1}H NMR, 77.16 ppm for ^{13}C NMR; DMSO-d_6: 2.50 ppm for ^{1}H NMR, 39.52 ppm for ^{13}C NMR;), all other NMR spectra externally to $SiMe_4$ (0 ppm). ^{1}H NMR chemical shifts are reported in ppm and coupling constants (J) are reported in Hertz (Hz). Abbreviations used for signal assignments: Ph = phenyl, Py = pyridyl, Py^{n} = non-coordinated pyridine, s = singlet, d = doublet, t = triplet, q = quartet, dd = doublet of doublets, m = multiplet, br = broad. NMR solvents were purchased from Cambridge Isotopes Laboratories and used as received. Ethylene gas was purchased from Matheson. Elemental analyses were performed using a Perkin-Elmer Model 2400 CHN analyzer. 4-t-Butylphenyl dibromoborane[1] and mesityl copper[2] were prepared according to literature procedures. All other reagents were obtained from commercial sources and used as received. Silver and gold complexes were prepared in reaction vessels protected from light using aluminum foil.

Synthesis of [*t*-BuPhB{2-(6-(CF_3)Py)}$_3$]H

To a solution of i-PrMgCl in THF (60.84 mL, 121.68 mmol, 2M), a solution of 2-bromo-6-(trifluoromethyl)pyridine in 55 mL THF (25.0 g, 110.62 mmol) was slowly added through a syringe at 0 °C. The resulting dark brown reaction mixture was warmed to room temperature and kept stirring for 5 h. The solvent was reduced under vacuum to obtain the dark slurry, which was then carefully transferred under nitrogen protection to a fritted addition funnel and anhydrous THF (ca. 50 mL) was used to help complete the transfer of the solids. Anhydrous THF was continuously passed through the filter cake until it was white and the filtrate colorless. The solid was dried under high vacuum at room temperature for 6 h and then further dried under high vacuum at 65 °C for 6 h. We assumed the resulted Grignard formed as {(6-(CF_3)-2-Py)MgCl}$_2$•(THF)$_3$. Yield, 15 g (38 %).

t-Butylphenyl dibromoborane (3.00 g, 9.87 mmol) in CH_2Cl_2 (20 mL) was added dropwise to a solution of {(6-(CF_3)-2-Py)MgCl}$_2$•(THF)$_3$ (9.3 g, 14.81 mmol) in CH_2Cl_2 (20 mL) at 0 °C. The resulting dark red mixture was slowly warmed to room temperature and kept stirring for 48 h. The reaction mixture was then poured into an aqueous Na_2CO_3 solution (18.0 g in 150 mL H_2O) and stirred for 1h, and then extracted with CH_2Cl_2 (3 × 30 mL). The organic extracts were combined, washed with brine, dried over Na_2SO_4 and evaporated to dryness. The residue

dissolved in CH_2Cl_2 (50 mL), activated charcoal was added and then filtered through small pad of Celite and evaporated to dryness. The resulting residue was recrystallized from acetone to obtain the desired **[*t*-BuPhB{2-(6-(CF_3)Py)}$_3$]H** as white crystalline solid. Yield: 4.96 g (86%). Anal. Calc. $C_{28}H_{23}B_1F_9N_3$: C, 57.66%; H, 3.97%; N, 7.20%. Found: C, 57.73%; H, 4.05%; N, 7.15%. ^{1}H NMR (500 MHz, $CDCl_3$): δ = 19.11 (br, 1H, NH), 7.74 – 7.69 (m, 6H, Py), 7.50 (d, *J* = 6.9 Hz, 3H, Py), 7.21 (d, *J* = 7.8 Hz, 2H, Ph), 7.04 (d, *J* = 7.0 Hz, 2H, Ph), (s, 9H, CH_3) ppm. ^{11}B NMR (96 MHz, $CDCl_3$): δ = -11.56 ppm. ^{13}C NMR (126 MHz, $CDCl_3$): δ = 184.79 (q, $^1J_{C-B}$ = 55.2 Hz, Py), 150.15(q, $^1J_{C-B}$ = 54.0 Hz, Ph), 147.86 (Ph), 142.60 (q, $^2J_{C-F}$ = 36.0 Hz, Py), 136.55 (Py), 134.60 (Py), 134.44 (Ph), 124.53 (Ph), 121.5 (q, $^1J_{C-F}$ = 274.7 Hz, CF_3), 117.16 (Py), 34.38 (C-CH_3), 31.59 (CH_3). ^{19}F NMR (471 MHz, $CDCl_3$): δ = -67.40 ppm. ^{11}B NMR, $CDCl_3$): δ = -11.56 ppm. This product was further characterized by X-ray crystallography.

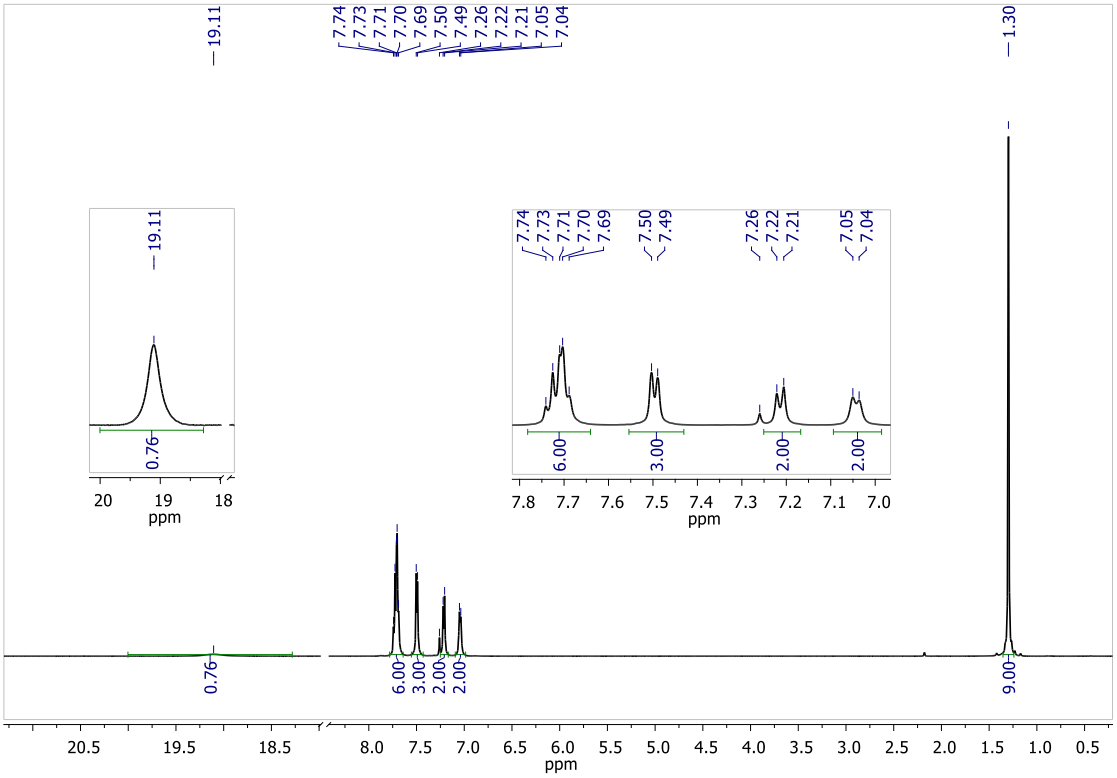

Figure S1. ^{1}H NMR spectrum of **[*t*-BuPhB{2-(6-(CF$_3$)Py)}$_3$]H** in $CDCl_3$

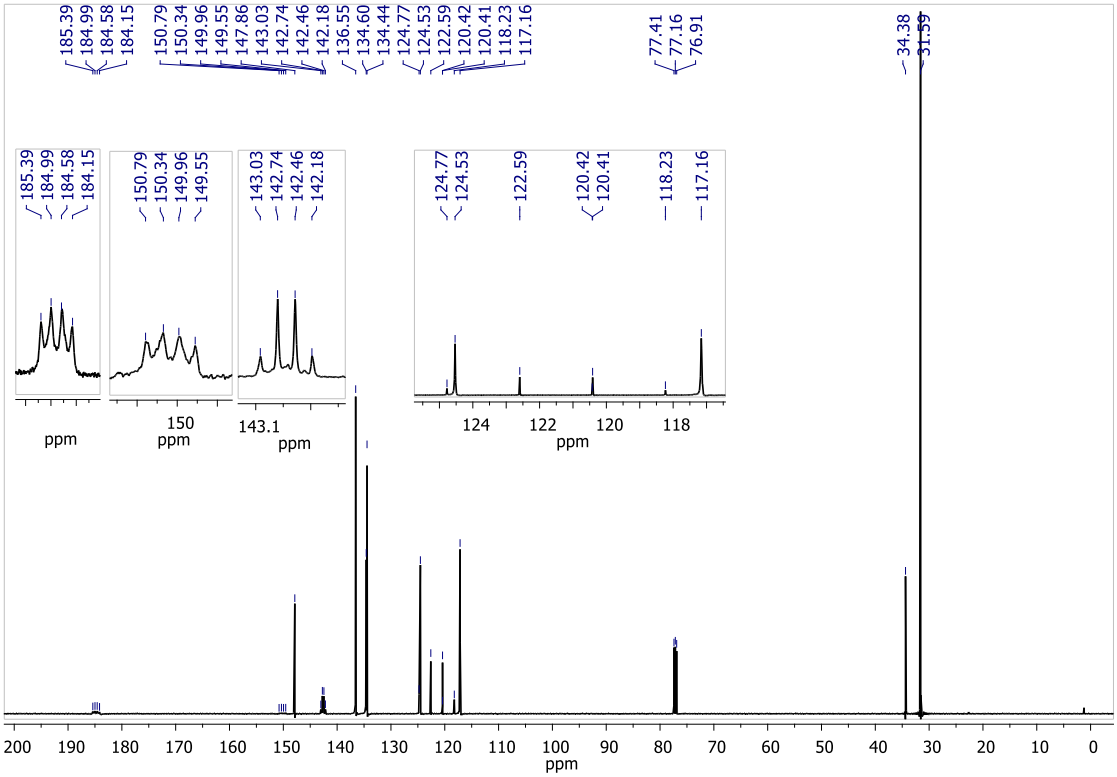

Figure S2. ^{13}C NMR spectrum of **[*t*-BuPhB{2-(6-(CF$_3$)Py)}$_3$]H** in $CDCl_3$

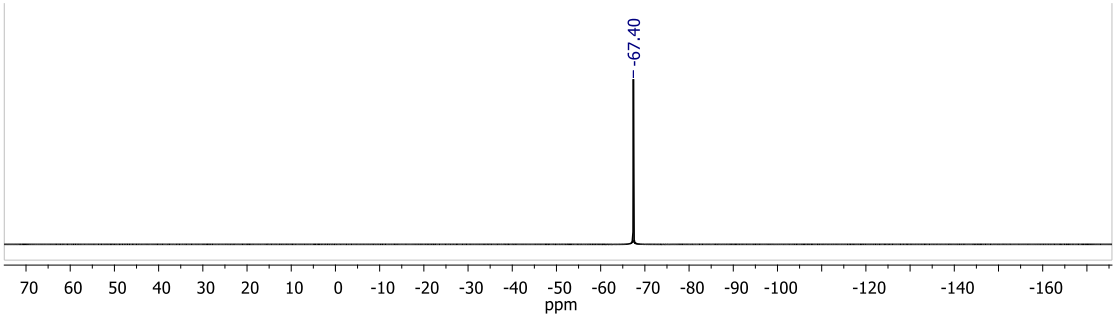

Figure S3. ^{19}F NMR spectrum of **[*t*-BuPhB{2-(6-(CF$_3$)Py)}$_3$]H** in $CDCl_3$

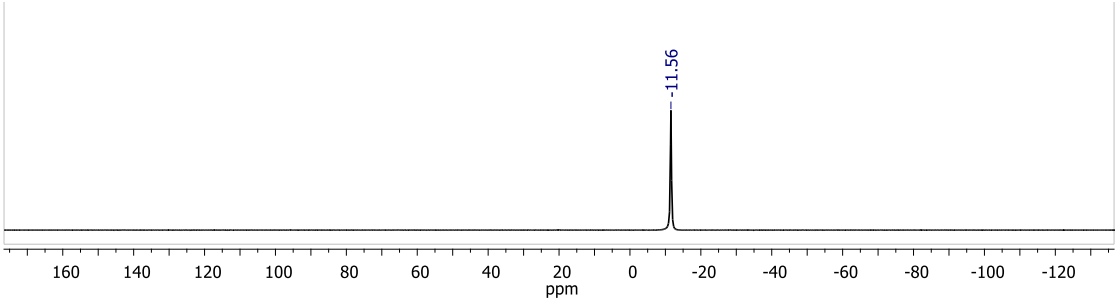

Figure S4. ^{11}B NMR spectrum of **[*t*-BuPhB{2-(6-(CF$_3$)Py)}$_3$]H** in $CDCl_3$

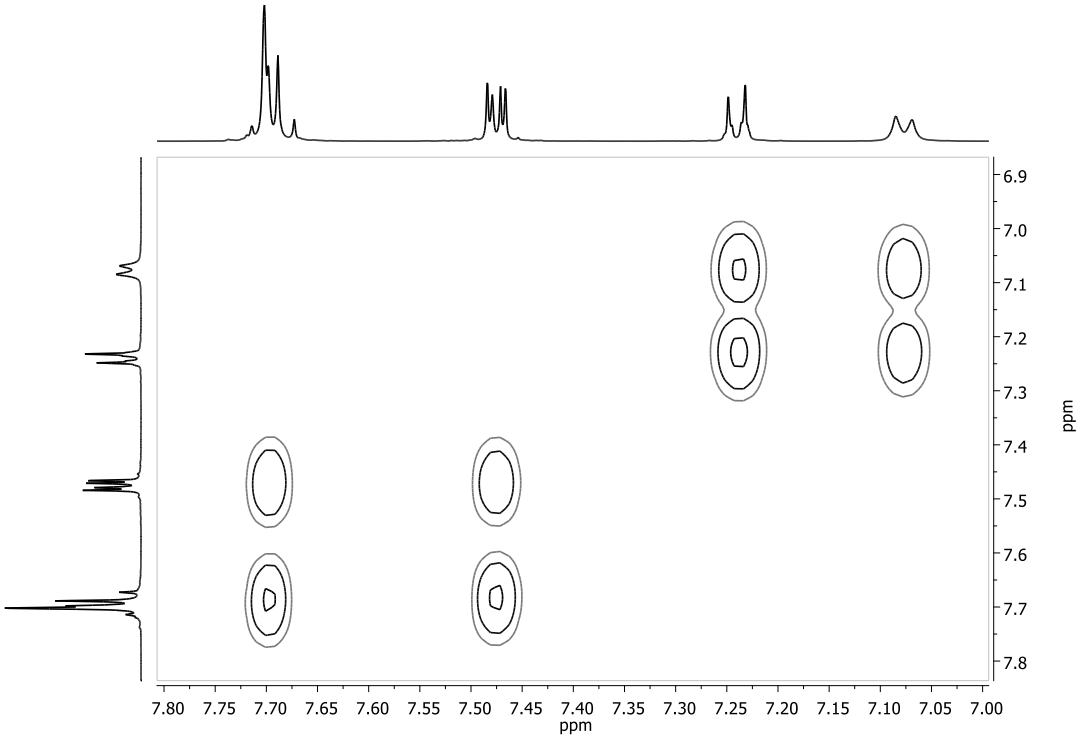

Figure S5. COSY NMR spectrum of **[*t*-BuPhB{2-(6-(CF_3)Py)}$_3$]H** in $CDCl_3$

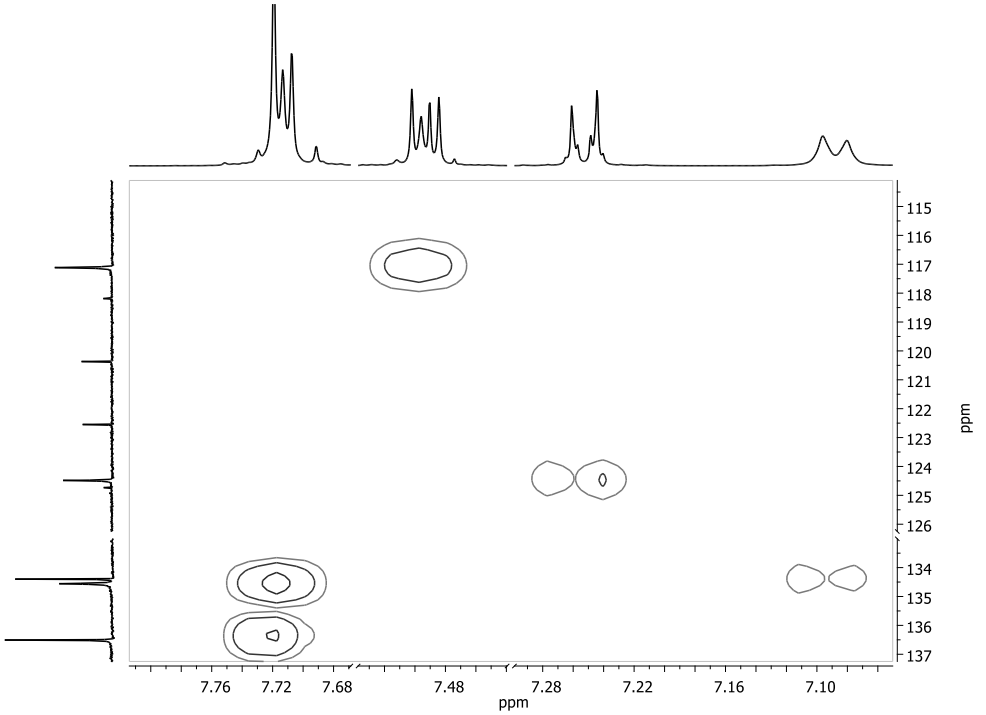

Figure S6. HSQC NMR spectrum of **[*t*-BuPhB{2-(6-(CF_3)Py)}$_3$]H** in $CDCl_3$

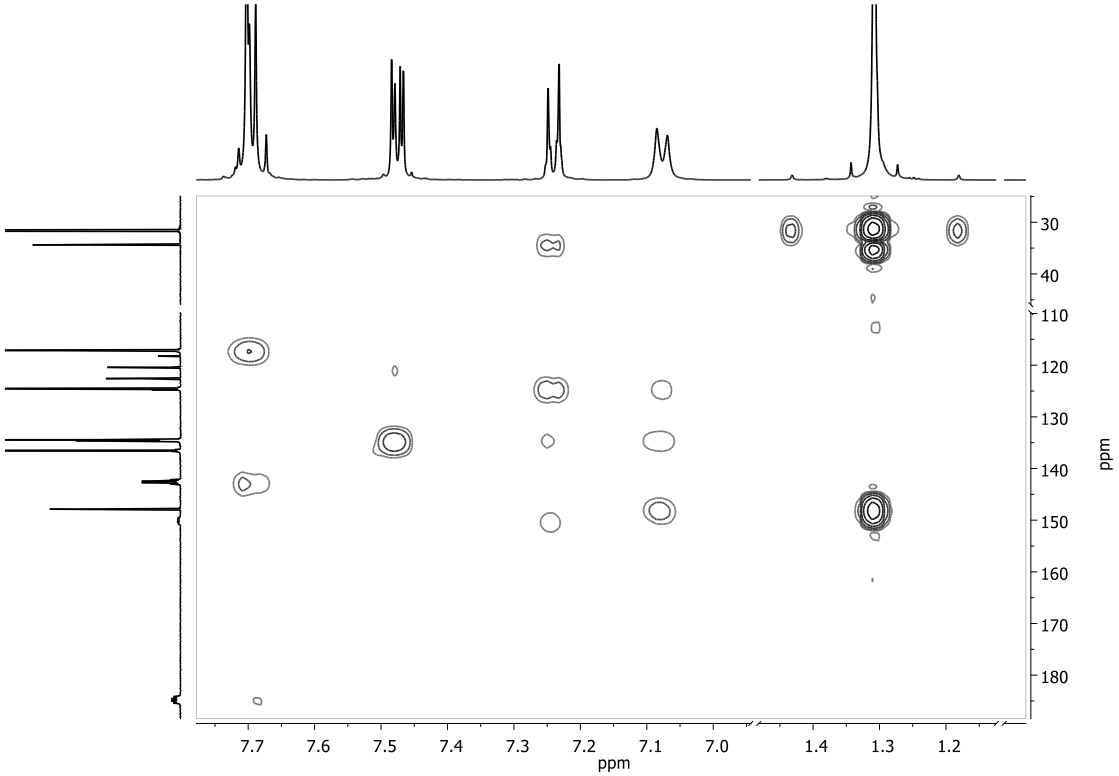

Figure S7. HMBC NMR spectrum of **[*t*-BuPhB{2-(6-(CF_3)Py)}$_3$]H** in $CDCl_3$

Synthesis of [*t*-BuPhB{2-(6-(CF$_3$)Py)}$_3$]K

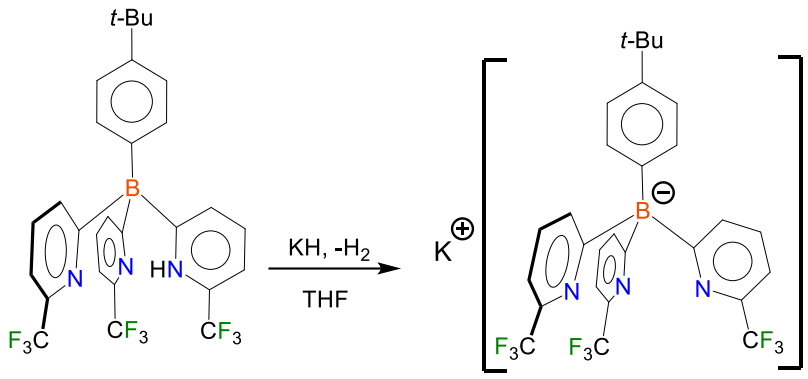

To a suspension of KH (0.23 g, 5.71 mmol) in anhydrous THF (25 mL) at 0 °C was slowly added a solution of [*t*-BuPhB{2-(6-(CF$_3$)Py)}$_3$]H (2.56 g, 4.39 mmol) in THF (25 mL). After complete ceasing of hydrogen gas evolution, the reaction mixture was allowed to warm to room temperature and then kept stirring for 12 h. The solution was filtered through a celite packed frit to remove unreacted KH. The solvent in the filtrate collected was removed under reduced pressure to obtain **[*t*-BuPhB{2-(6-(CF$_3$)Py)}$_3$]K** as a white solid. The compound was further dried at 90 °C for 6 h under reduced pressure to remove all trace solvent. Yield: 2.57 (94%). This was used directly in the next steps. ^{1}H NMR (500 MHz, DMSO-d$_6$): δ = 7.62 (d, J = 7.9 Hz, 3H, Py), 7.49 (t, J = 7.8 Hz, 3H, Py), 7.28 (dd, J = 7.6, 1.0 Hz, 3H, Py), 7.14 (d, J = 5.4 Hz, 2H, Ph), 6.99 (d, J = 8.3 Hz, 2H, Ph), 1.23 (s, 9H, CH$_3$) ppm. ^{13}C NMR (126 MHz, MHz, DMSO-d$_6$): δ = 188.25 (q, $^1J_{C\text{-}B}$ = 55.2 Hz, Py), 155.82 (q, $^1J_{C\text{-}B}$ = 50.4 Hz, Ph), 144.39 (q, $^2J_{C\text{-}F}$ = 31.2 Hz, Py), 144.16 (Ph), 134.65 (Ph), 132.88 (Py), 132.48 (Py), 122.82 (q, $^1J_{C\text{-}F}$ = 274.7 Hz, CF$_3$), 122.56 (Ph), 114.05 (Py), 33.74 (C-CH$_3$), 31.54 (CH$_3$). ^{19}F NMR (471 MHz, DMSO--d$_6$): δ = -66.18 ppm. ^{11}B NMR (96 MHz, DMSO-d$_6$): δ = -8.35 ppm.

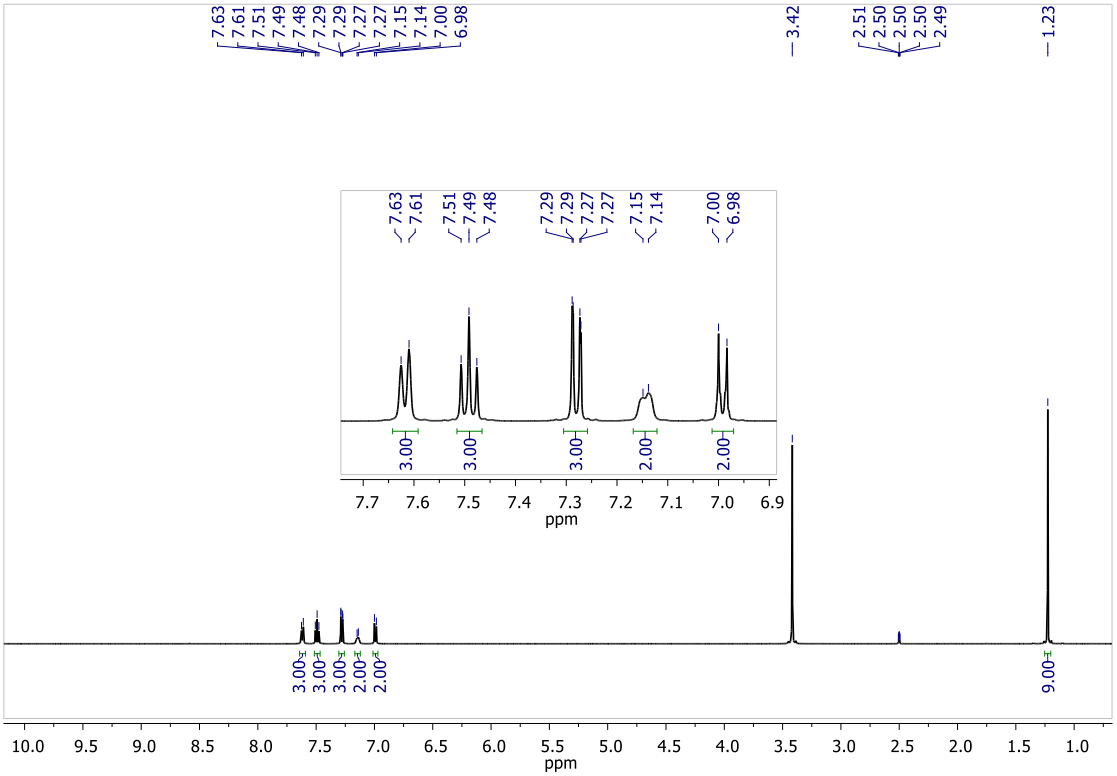

Figure S8. ^{1}H NMR spectrum of **[*t*-BuPhB{2-(6-(CF$_3$)Py)}$_3$]K** in DMSO-d$_6$

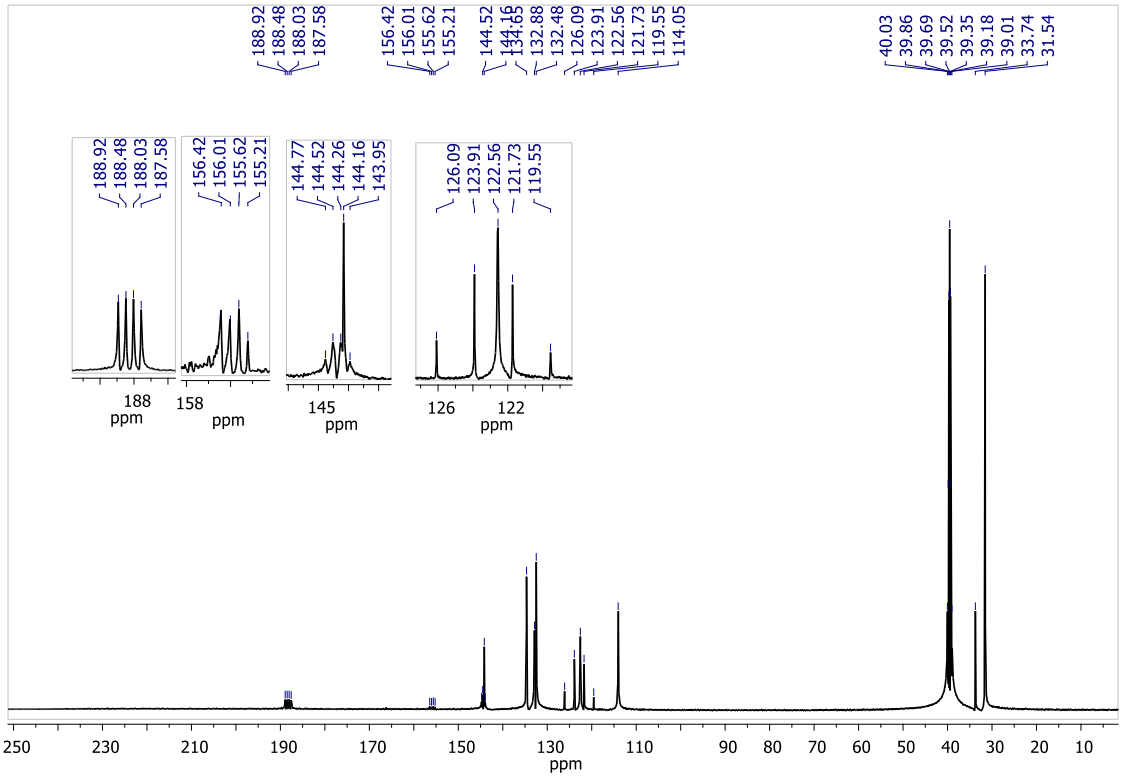

Figure S9. ^{13}C NMR spectrum of **[*t*-BuPhB{2-(6-(CF$_3$)Py)}$_3$]K** in DMSO-d$_6$

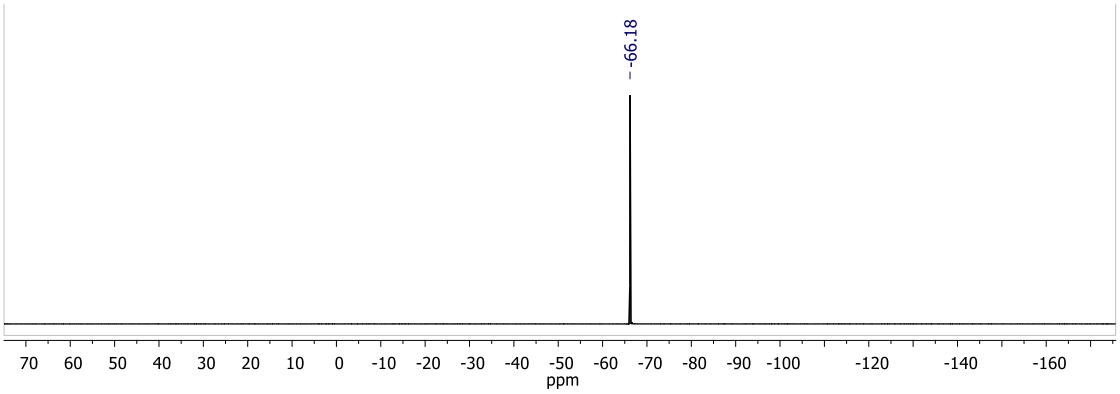

Figure S10. ^{19}F NMR spectrum of **[*t*-BuPhB{2-(6-(CF$_3$)Py)}$_3$]K** in DMSO-d$_6$

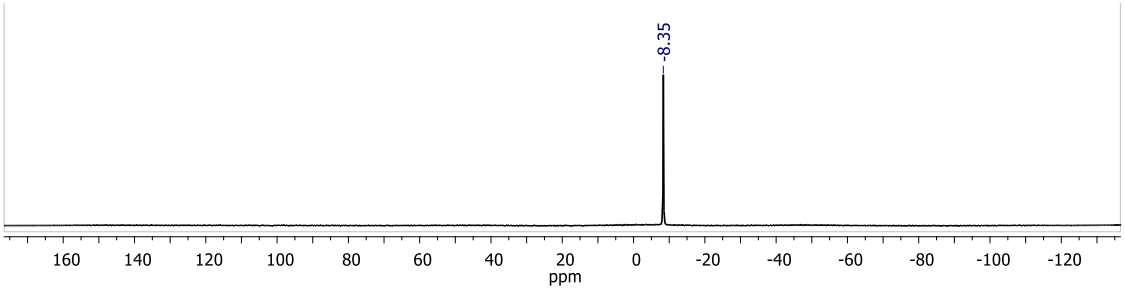

Figure S11. ^{11}B NMR spectrum of **[*t*-BuPhB{2-(6-(CF$_3$)Py)}$_3$]K** in DMSO-d$_6$

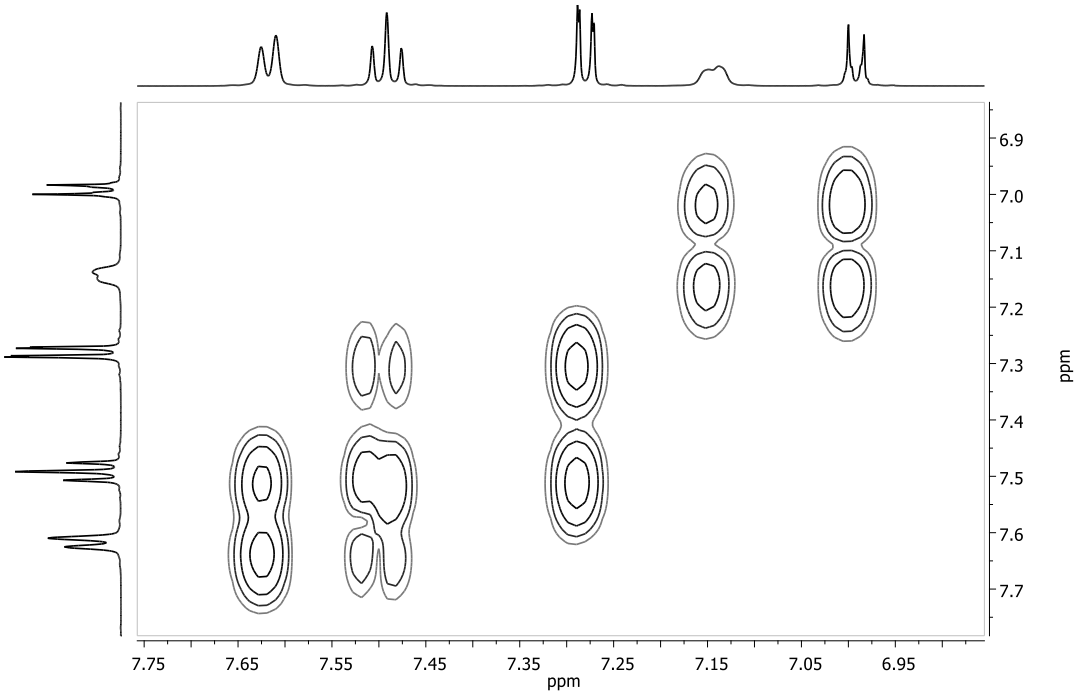

Figure S12. COSY NMR spectrum of **[*t*-BuPhB{2-(6-(CF$_3$)Py)}$_3$]K** in DMSO-d$_6$

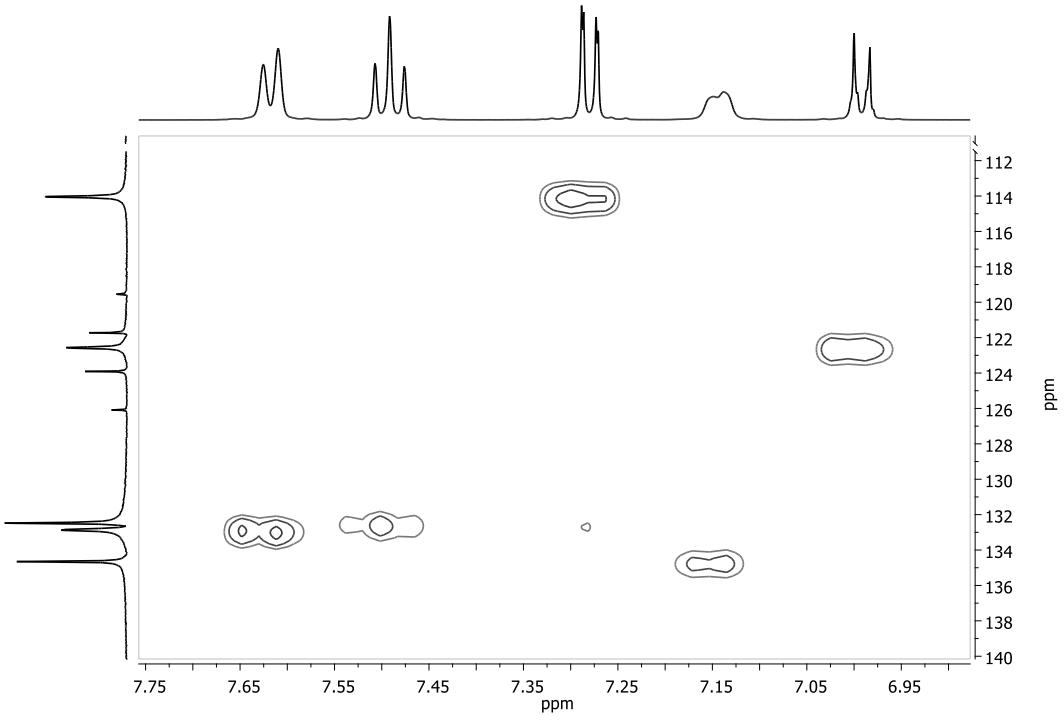

Figure S13. HSQC NMR spectrum of **[*t*-BuPhB{2-(6-(CF$_3$)Py)}$_3$]K** in DMSO-d$_6$

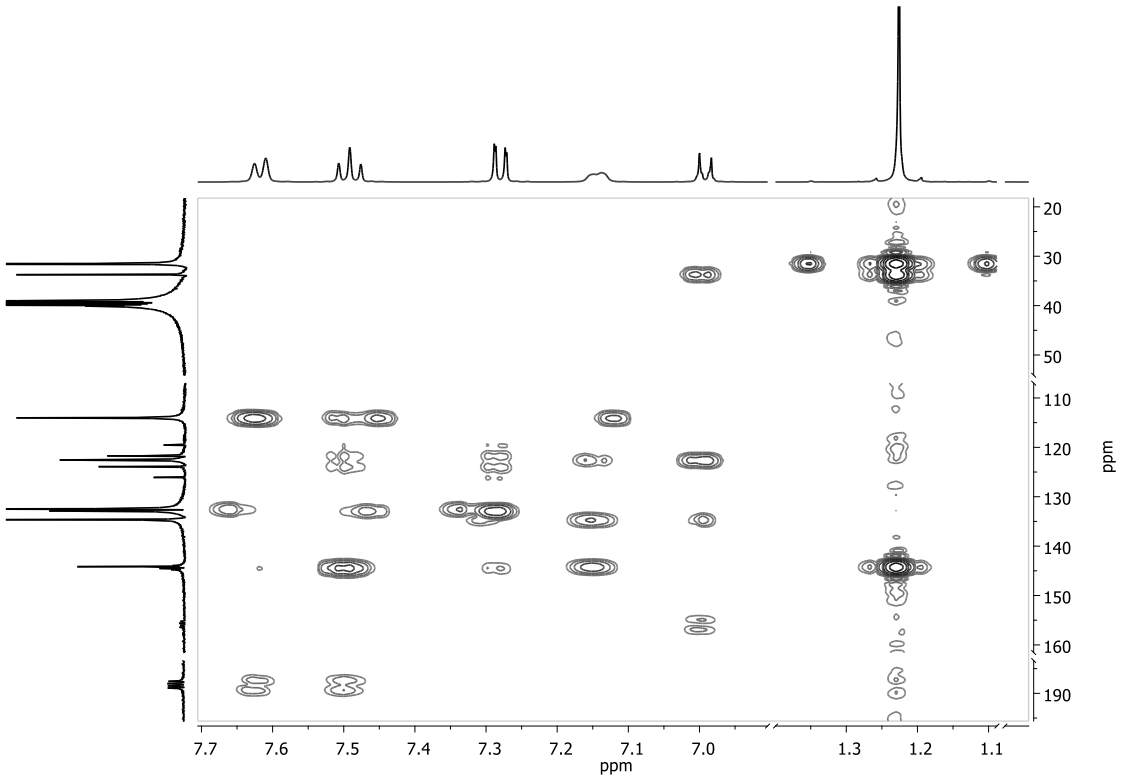

Figure S14. HMBC NMR spectrum of **[*t*-BuPhB{2-(6-(CF_3)Py)}$_3$]K** in DMSO-d_6

Synthesis of [*t*-BuPhB(6-(CF$_3$)Py)$_3$]Cu(C$_2$H$_4$)

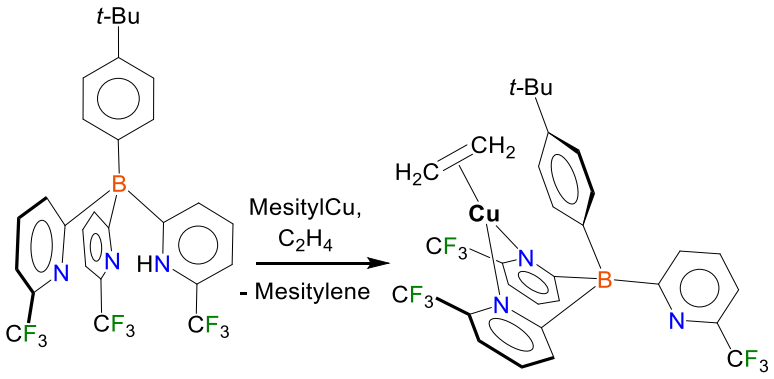

Ethylene saturated anhydrous toluene (15 mL) was transferred using a cannular to a 50 mL Schlenk flask containing a mixture of [*t*-BuPhB{2-(6-(CF$_3$)Py)}$_3$]H (150 mg, 257 mmol) and mesityl copper (52 mg, 282 mmol) at room temperature under ethylene atmosphere. The reaction mixture was kept stirring for 3h, during this period ethylene was bubbled every one hour for 30 seconds each time. The solvent was then removed reduced pressure, and the compound was recrystallized from ethylene saturated hexane at -20 °C to obtain colorless X-ray quality single crystals of [*t*-BuPhB{2-(6-(CF$_3$)Py)}$_3$]Cu(C$_2$H$_4$). Yield: 156 mg (90%). Anal. Calc. $C_{30}H_{26}B_1Cu_1F_9N_3$: C, 53.47%; H, 3.89%; N, 6.24%. Found: C, 52.62%; H, 3.82%; N, 6.05%. ^{1}H NMR (500 MHz, $CDCl_3$): δ = 7.86 (d, *J* = 7.9 Hz, 2H, Py), 7.67 (t, *J* = 7.9 Hz, 2H, Py), 7.57 (t, *J* = 7.8 Hz, 1H, Py^n), 7.48 (two overlapped doublets, 1H, Py^n; 2H, Py), 7.21 (d, *J* = 8.2 Hz, 2H, Ph), 6.95 (d, *J* = 7.7 Hz, 1H, Py^n), 6.76 (d, *J* = 6.0 Hz, 2H, Ph), 3.57 (s, 4H, C_2H_4), 1.30 (s, 9H, CH_3) ppm. ^{13}C NMR (126 MHz, $CDCl_3$): δ = 185.98 (q, $^1J_{C\text{-}B}$ = 52.8 Hz, Py), 182.14 (q, $^1J_{C\text{-}B}$ = 57.6 Hz, Py^n),, 150.28 (q, $^1J_{C\text{-}B}$ = 50.4 Hz, Ph), 149.39 (Ph), 146.77 (q, $^2J_{C\text{-}F}$ = 33.6 Hz, Py^n), 145.77 (q, $^2J_{C\text{-}F}$ = 33.6 Hz, Py), 137.35 (Ph), 136.00 (Py), 135.23 (Py^n), 133.95 (Py), 133.59 (Py^n), 124.66 (Ph), 122.68 (q, $^1J_{C\text{-}F}$ = 274.7 Hz, CF_3-Py), 121.96 (q, $^1J_{C\text{-}F}$ = 274.7 Hz, CF_3- Py^n), 117.97 (Py), 115.95 (Py^n), 85.13 (C_2H_4), 34.56 (C-CH_3), 31.53 (CH_3) ppm. ^{19}F NMR (471 MHz, $CDCl_3$): δ = -65.57 (s, 6F, CF_3-Py), -67.85(s, 3F, CF_3- Py^n) ppm. ^{11}B NMR (96 MHz, $CDCl_3$): δ = -8.47 ppm.

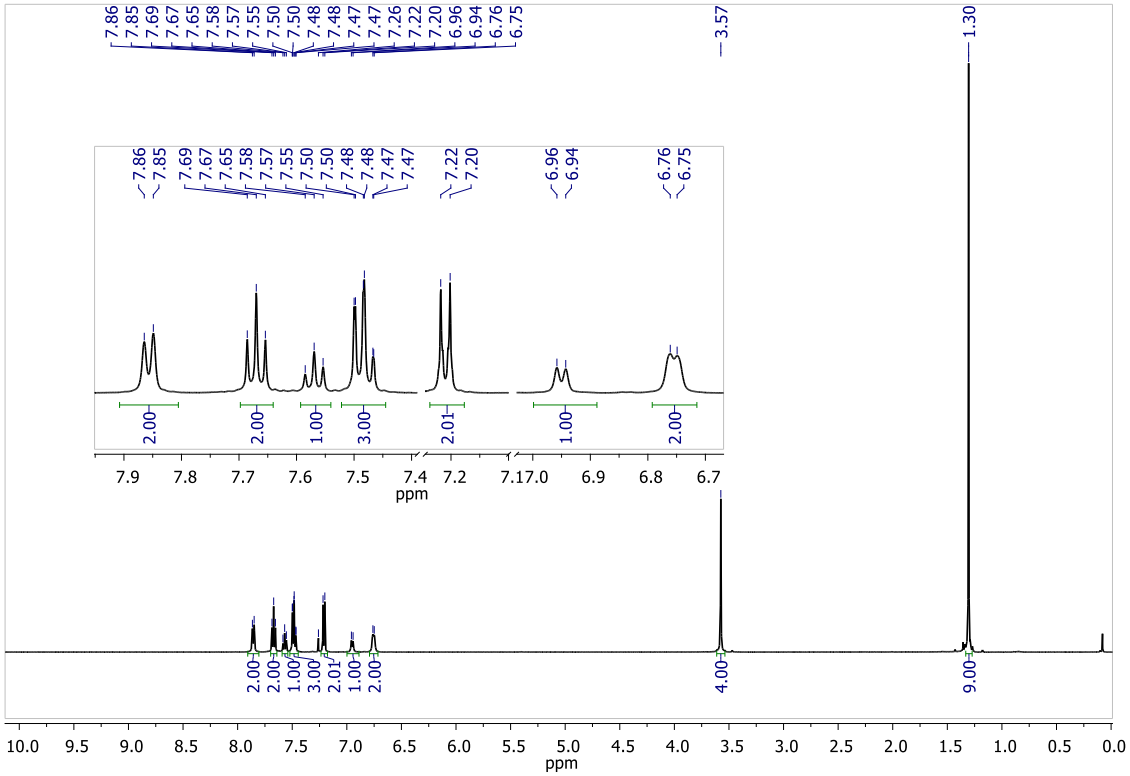

Figure S15. ^{1}H NMR spectrum of **[*t*-BuPhB{2-(6-(CF$_3$)Py)}$_3$]Cu(C$_2$H$_4$)** in $CDCl_3$

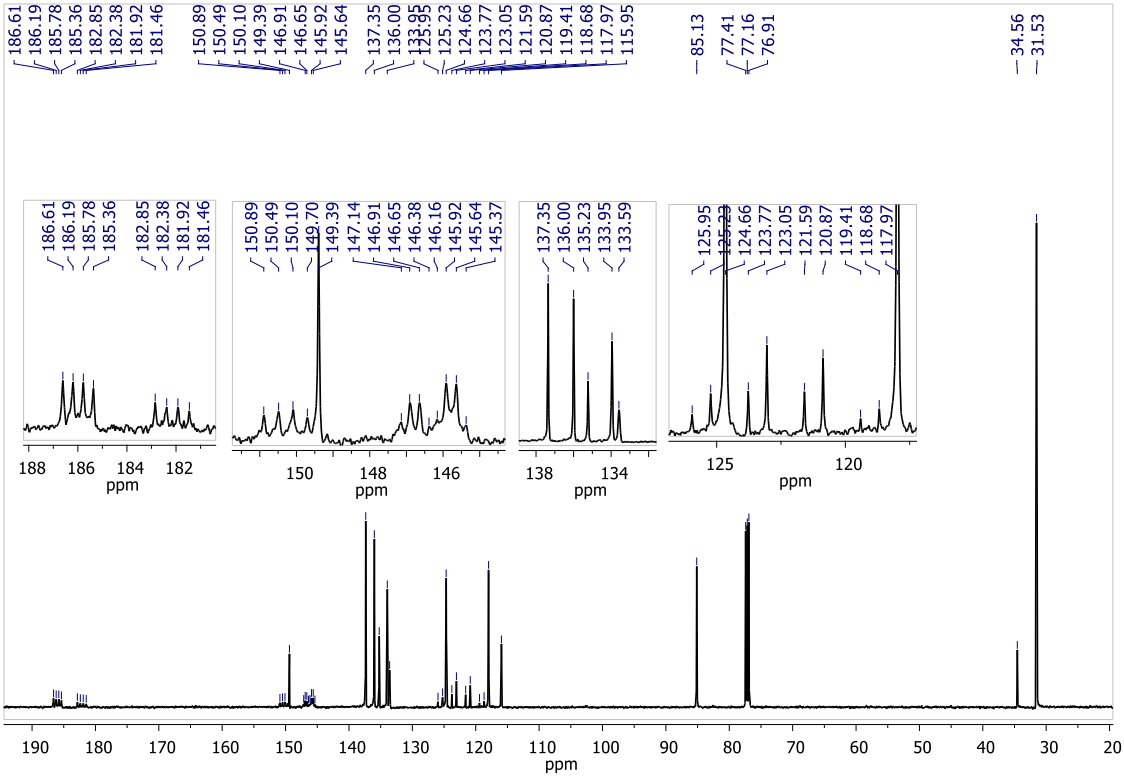

Figure S16. ^{13}C NMR spectrum of **[*t*-BuPhB{2-(6-(CF_3)Py)}$_3$]Cu(C_2H_4)** in $CDCl_3$

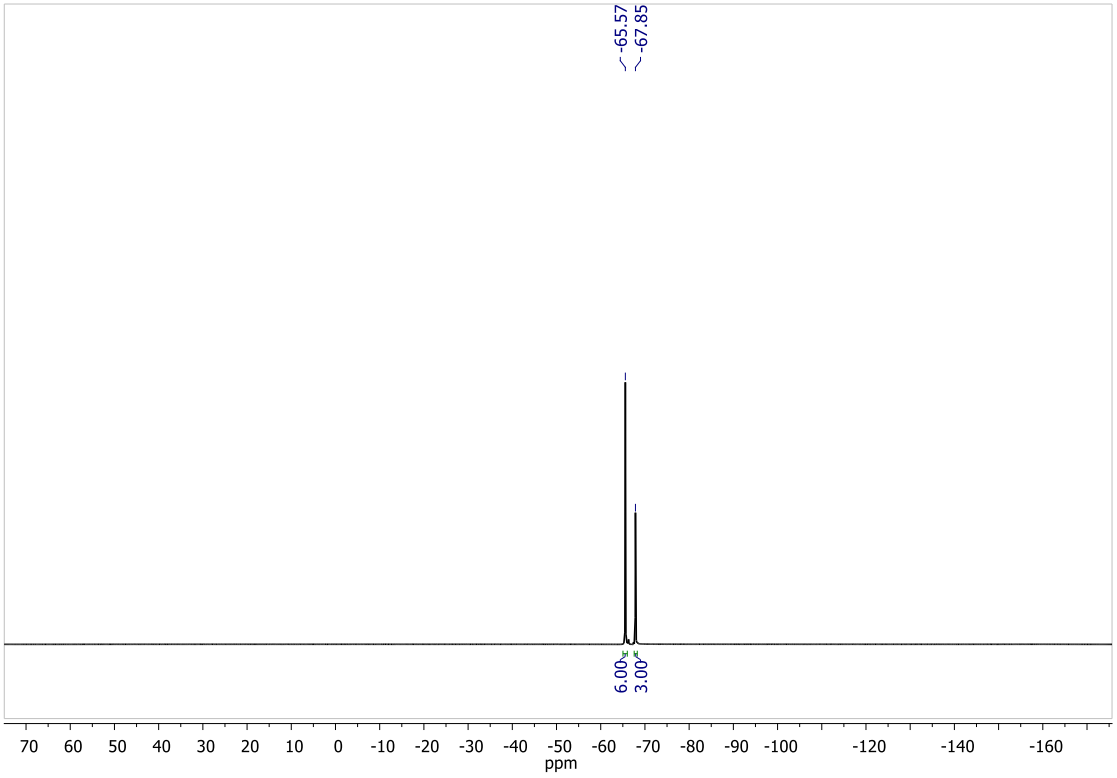

Figure S17. ^{19}F NMR spectrum of **[*t*-BuPhB{2-(6-(CF$_3$)Py)}$_3$]Cu(C$_2$H$_4$)** in CDCl$_3$

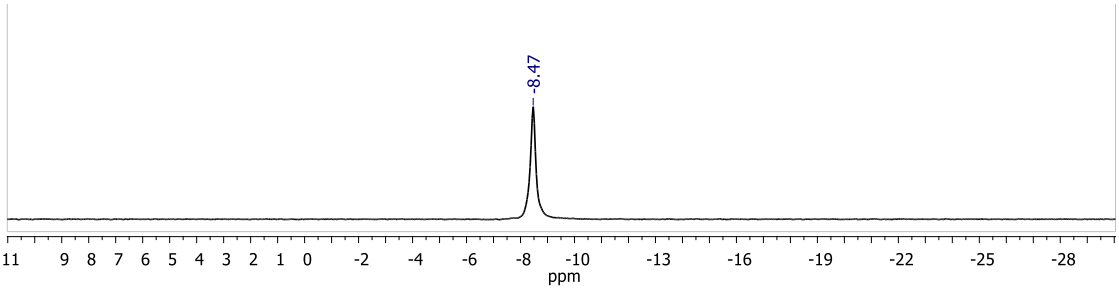

Figure S18. ^{11}B NMR spectrum of **[*t*-BuPhB{2-(6-(CF$_3$)Py)}$_3$]Cu(C$_2$H$_4$)** in CDCl$_3$

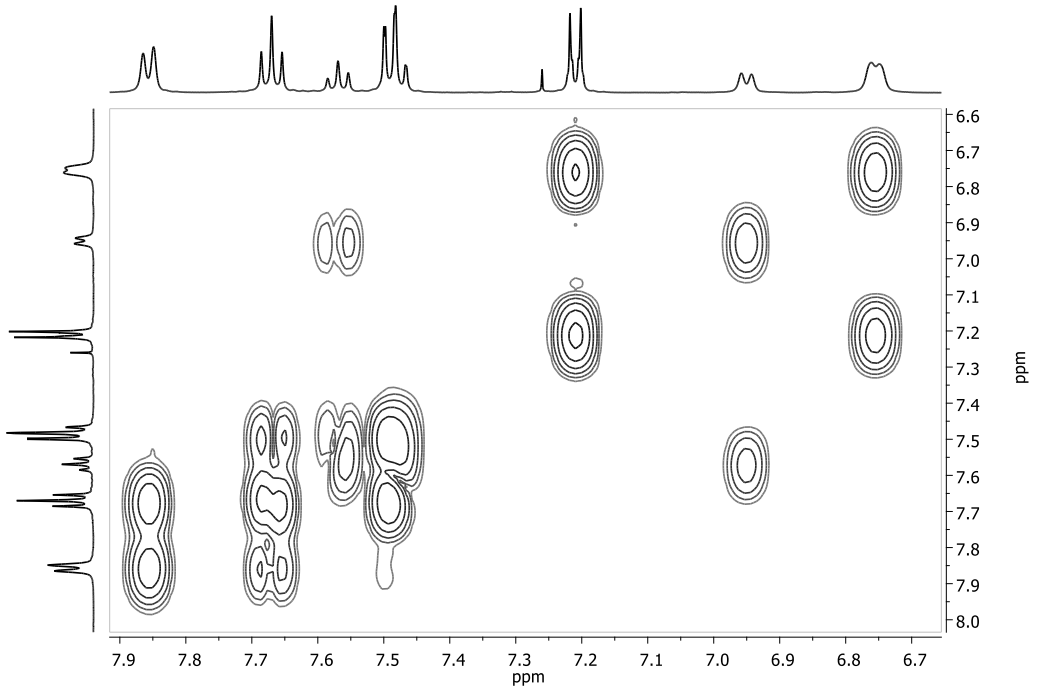

Figure S19. COSY NMR spectrum of **[*t*-BuPhB{2-(6-(CF_3)Py)}$_3$]Cu(C_2H_4)** in $CDCl_3$

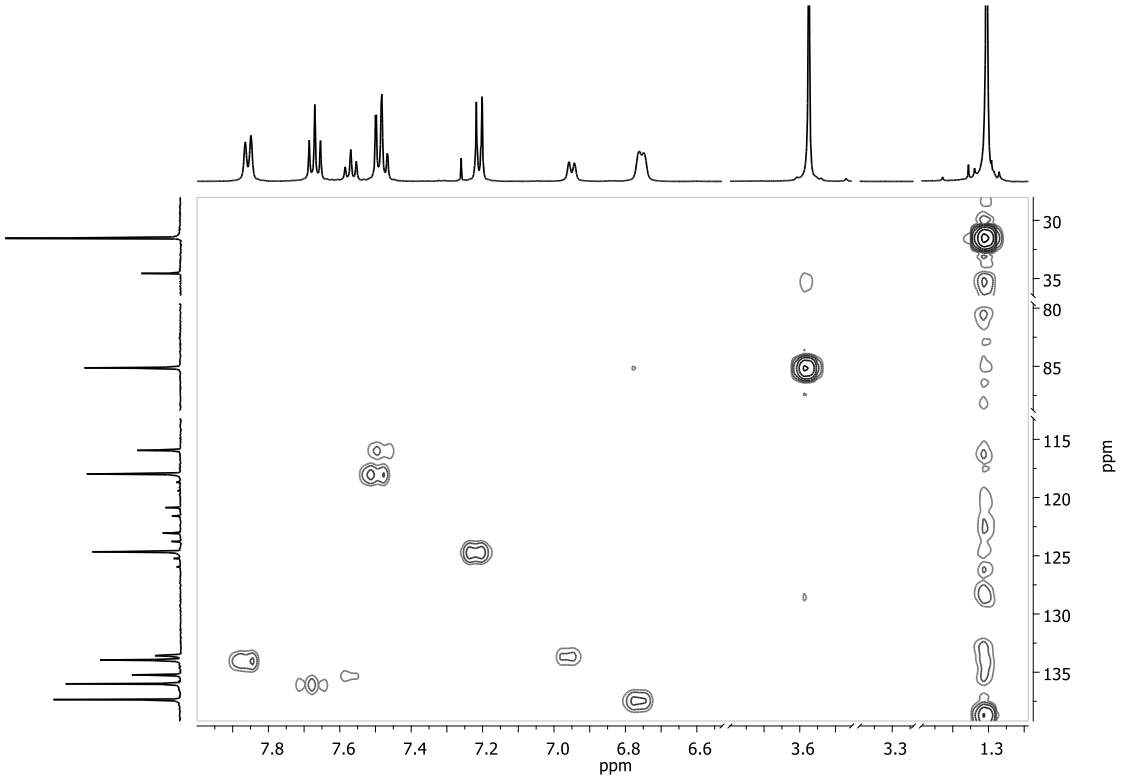

Figure S20. HSQC NMR spectrum of **[*t*-BuPhB{2-(6-(CF_3)Py)}$_3$]Cu(C_2H_4)** in $CDCl_3$

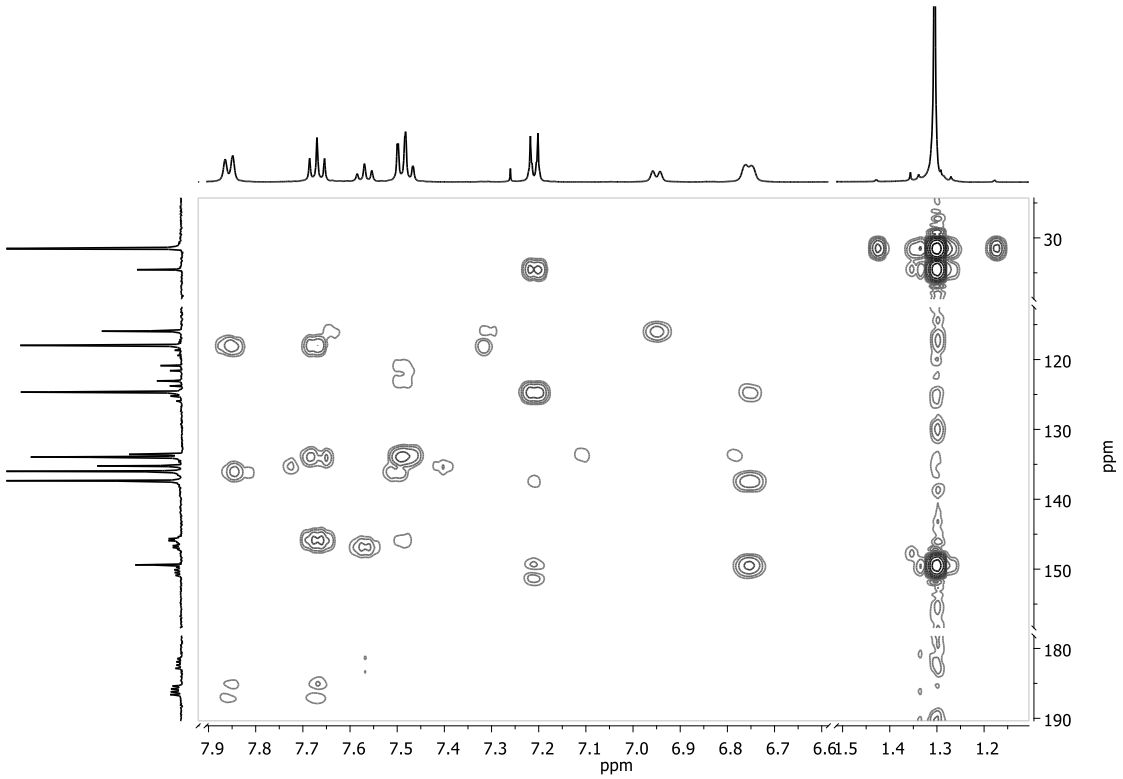

Figure S21. HMBC NMR spectrum of **[*t*-BuPhB{2-(6-(CF_3)Py)}$_3$]Cu(C_2H_4)** in $CDCl_3$

Synthesis of [*t*-BuPhB{2-(6-(CF$_3$)Py)}$_3$]Ag(C$_2$H$_4$)

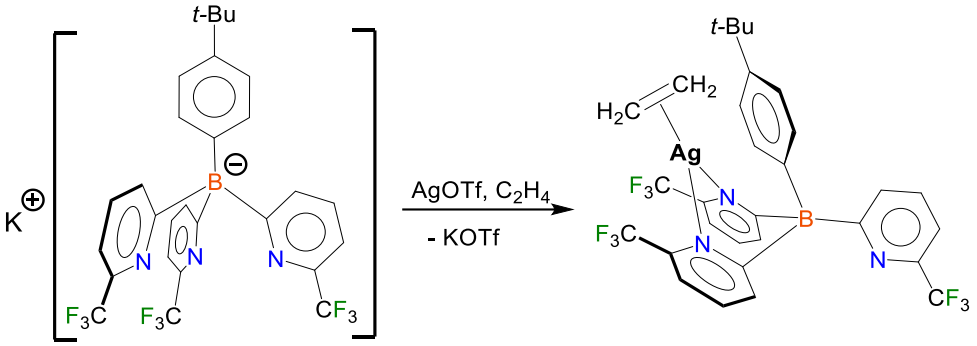

Ethylene saturated anhydrous dichloromethane (15 mL) was transferred using a cannular to a 50 mL Schlenk flask containing a mixture of [*t*-BuPhB{2-(6-(CF$_3$)Py)}$_3$]K (150 mg, 241 mmol) and AgOTf (65 mg, 253 mmol) at room temperature under ethylene atmosphere. The reaction mixture was kept stirring for 3h, during this period ethylene was bubbled every one hour for 30 seconds each time. The reaction mixture was then cannula filtered through a celite packed frit to remove KOTf. The filtrate was concentrated to c.a. 3 mL under reduced pressure and then dried with a flow of ethylene gas to obtain the white colored solid, which was then recrystallized from ethylene saturated hexane at -20 °C to obtain colorless X-ray quality single crystals of **[*t*-BuPhB{2-(6-(CF$_3$)Py)}$_3$]Ag(C$_2$H$_4$).** Yield: 130 mg (78%). Anal. Calc. $C_{30}H_{26}Ag_1B_1F_9N_3$: C, 50.17%; H, 3.65%; N, 5.85%. Found: C, 49.90%; H, 3.58%; N, 5.65%. ^{1}H NMR (500 MHz, $CDCl_3$): δ = 8.25 (brs, Py), 7.57 (brs, 3H, Py), 7.41 (d, J = 7.8 Hz, 3H, Py), 7.28 (d, J = 8.2 Hz, 2H, Ph), 6.89 (brs, 2H, Ph), 4.66 (s, 4H, C_2H_4), 1.34 (s, 9H, CH_3) ppm. ^{13}C NMR (126 MHz, $CDCl_3$): δ = 185.43 (brs, $Py_{C\text{-}B}$), 148.94 (Ph), 148.29 (q, $^1J_{C\text{-}B}$ = 51.6 Hz, Ph), 145.85 (q, $^2J_{C\text{-}F}$ = 30.0 Hz, Py), 136.86 (Ph), 135.35 (Py), 133.38 (Py), 124.63 (Ph), 122.3 (q, $^1J_{C\text{-}F}$ = 267.5 Hz, CF_3), 116.33 (Py), 103.15 (C_2H_4), 34.55 (C-CH_3), 31.66 (CH_3) ppm. ^{19}F NMR (471 MHz, $CDCl_3$): δ = -67.85 ppm. ^{11}B NMR (96 MHz, $CDCl_3$): δ = -7.90 ppm.

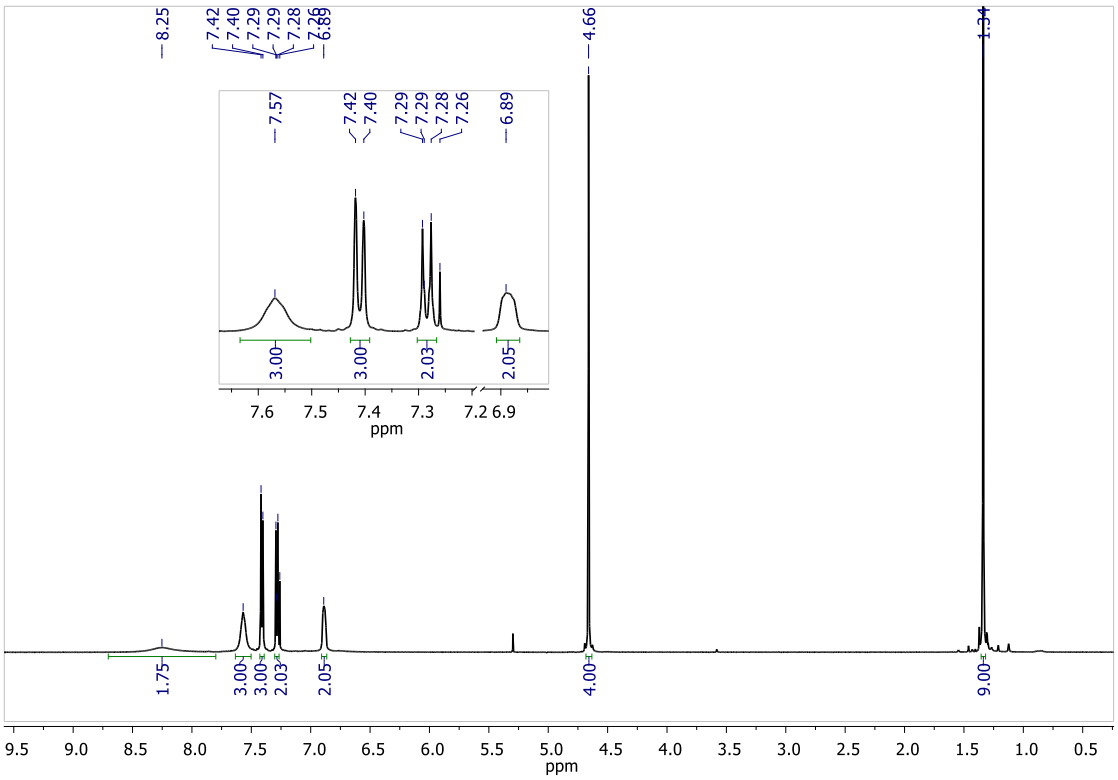

Figure S22. ^{1}H NMR spectrum of **[*t*-BuPhB{2-(6-(CF$_3$)Py)}$_3$]Ag(C$_2$H$_4$)** in $CDCl_3$

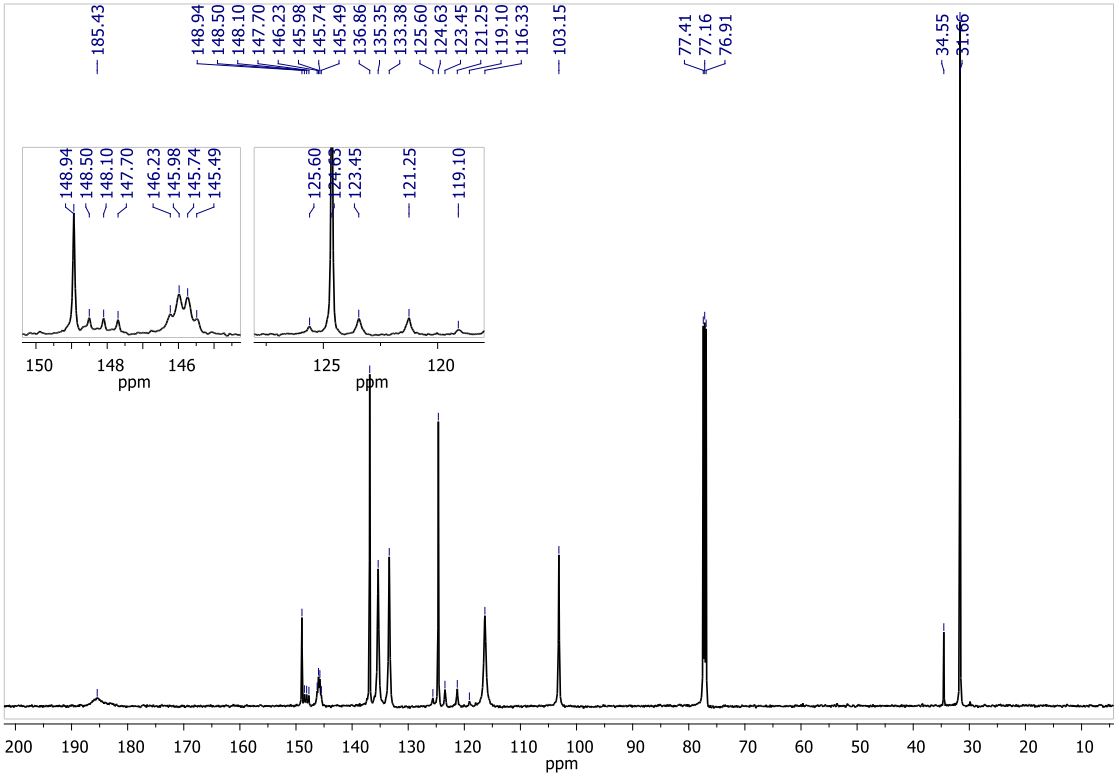

Figure S23. ^{13}C NMR spectrum of **[*t*-BuPhB{2-(6-(CF$_3$)Py)}$_3$]Ag(C$_2$H$_4$)** in CDCl$_3$

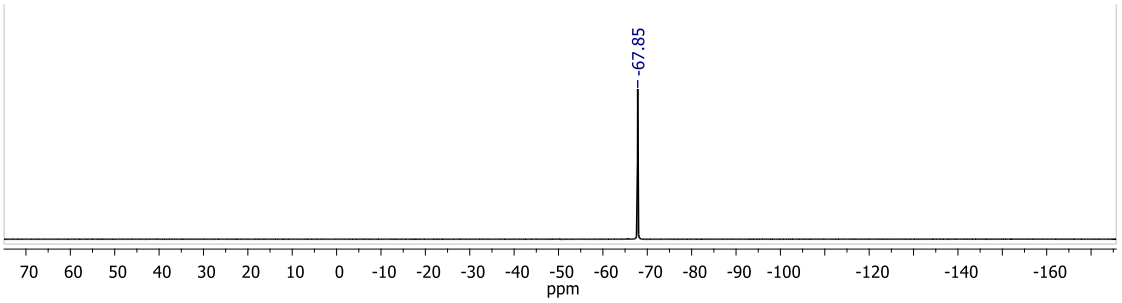

Figure S24. ^{19}F NMR spectrum of **[*t*-BuPhB{2-(6-(CF$_3$)Py)}$_3$]Ag(C$_2$H$_4$)** in $CDCl_3$

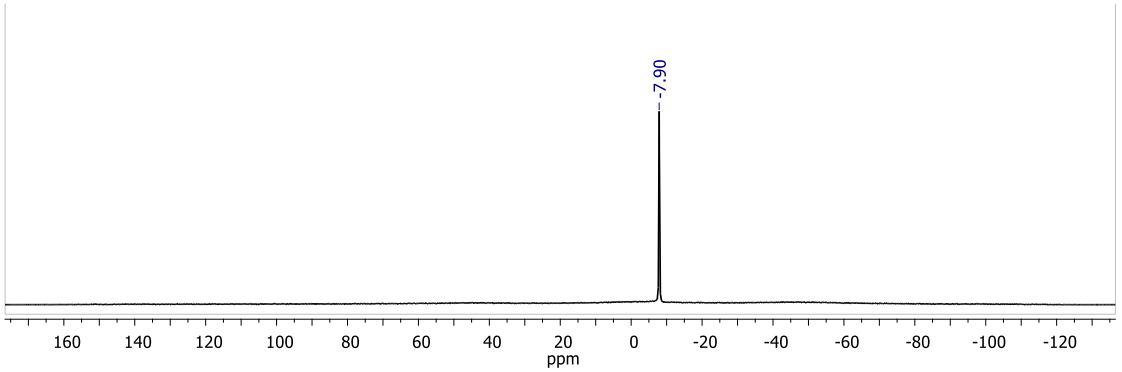

Figure S25. ^{11}B NMR spectrum of **[*t*-BuPhB{2-(6-(CF$_3$)Py)}$_3$]Ag(C$_2$H$_4$)** in $CDCl_3$

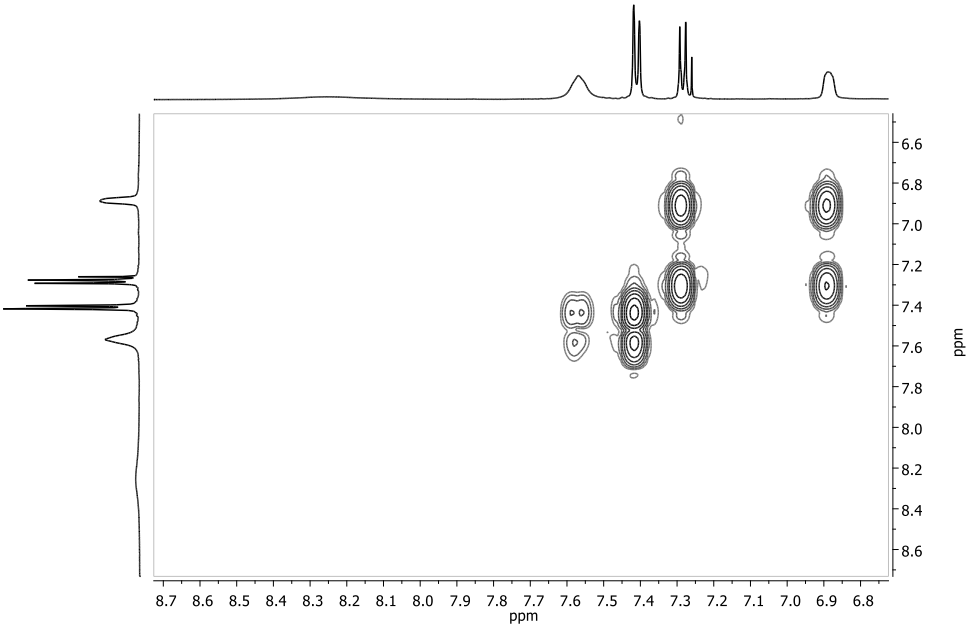

Figure S26. COSY spectrum of **[*t*-BuPhB{2-(6-(CF_3)Py)}$_3$]Ag(C_2H_4)** in $CDCl_3$

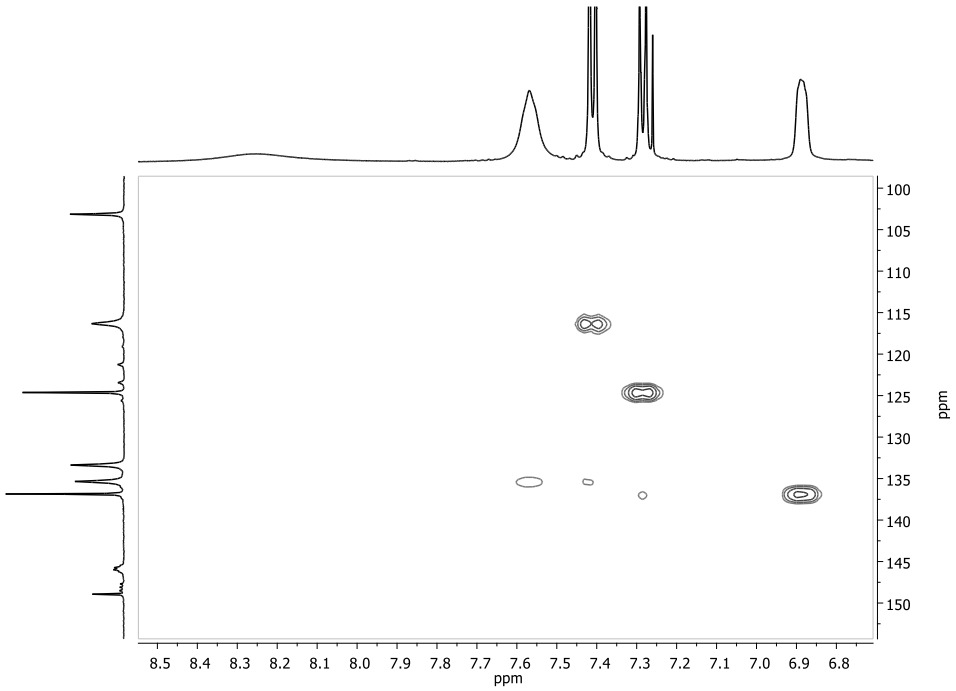

Figure S27. HSQC spectrum of **[*t*-BuPhB{2-(6-(CF_3)Py)}$_3$]Ag(C_2H_4)** in $CDCl_3$

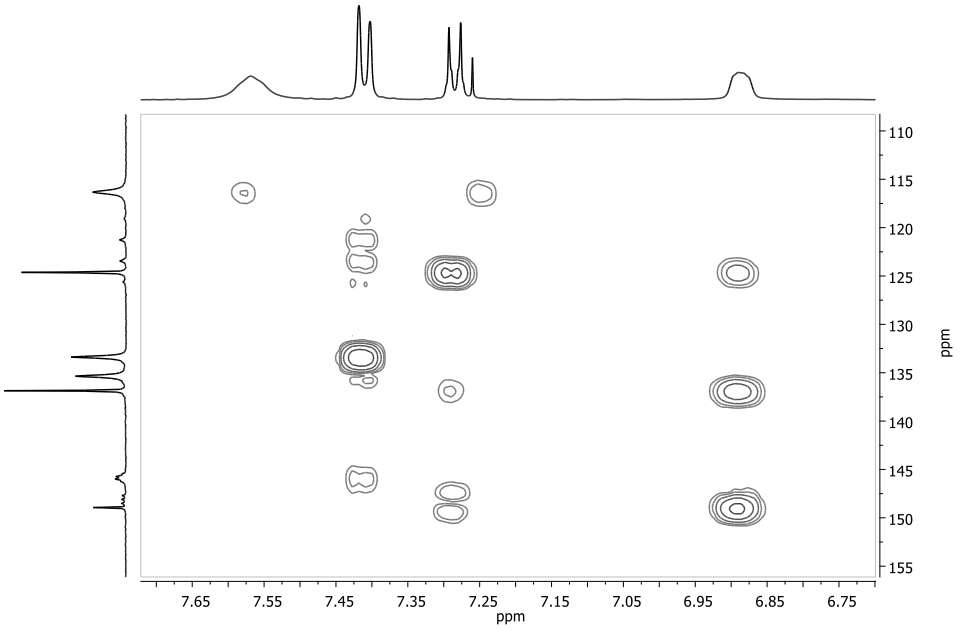

Figure S28. HMBC spectrum of **[*t*-BuPhB{2-(6-(CF_3)Py)}$_3$]Ag(C_2H_4)** in $CDCl_3$

Synthesis of [*t*-BuPhB{2-(6-(CF$_3$)Py)}$_3$]Au(C$_2$H$_4$)

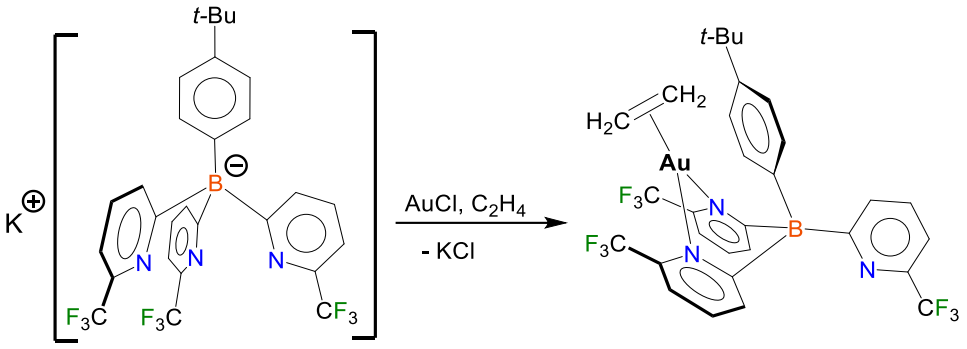

Ethylene saturated anhydrous dichloromethane (15 mL) at -78 °C was transferred using a cannular to a 50 mL Schlenk flask containing a mixture of [*t*-BuPhB{2-(6-(CF$_3$)Py)}$_3$]K (100 mg, 161 mmol) and AuCl (39 mg, 169 mmol) at -78 °C under ethylene atmosphere. After stirring 10 min at -78 °C, the reaction mixture then warmed to room temperature and stirred for another 10 min, then filtered through a celite-covered fritted funnel once the solution was colorless. The solvent was then removed under reduced pressure to obtain the white solid, which was then recrystallized from ethylene saturated hexane at -20 °C to obtain colorless X-ray quality single crystals of [*t*-BuPhB{2-(6-(CF$_3$)Py)}$_3$]Au(C$_2$H$_4$). Yield: 81 mg (62%). Anal. Calc. $C_{30}H_{26}Au_1B_1F_9N_3$: C, 44.63%; H, 3.25%; N, 5.20%. Found: C, 44.82%; H, 3.20%; N, 5.07%. ^{1}H NMR (500 MHz, $CDCl_3$): δ = 7.83 (brs, Py), 7.65 (t, J = 7.6 Hz, 3H, Py), 7.54 (d, J = 7.9 Hz, 3H, Py), 7.16 (d, J = 8.2 Hz, 2H, Ph), 6.65 (t, J = 11.8 Hz, 2H, Ph), 2.66 (s, 4H, C_2H_4), 1.29 (s, 9H, CH_3). ^{13}C NMR (126 MHz, $CDCl_3$): δ = 186.42 (brs, Py), 151.31 (q, $^1J_{C\text{-}B}$ = 50.4 Hz, Ph), 148.46 (Ph), 146.34 (q, $^2J_{C\text{-}F}$ = 33.6 Hz, Py), 136.10 (Ph), 135.84 (Py), 134.71 (Py), 124.08 (Ph), 121.5 (q, $^1J_{C\text{-}F}$ = 274.7 Hz, CF_3), 117.73 (Py), 58.67 (C_2H_4), 34.42 (C-CH_3), 31.64 (CH_3) ppm. ^{19}F NMR (471 MHz, $CDCl_3$): δ = -66.31, -67.53 ppm. ^{11}B NMR (96 MHz, $CDCl_3$): δ = -8.18 ppm.

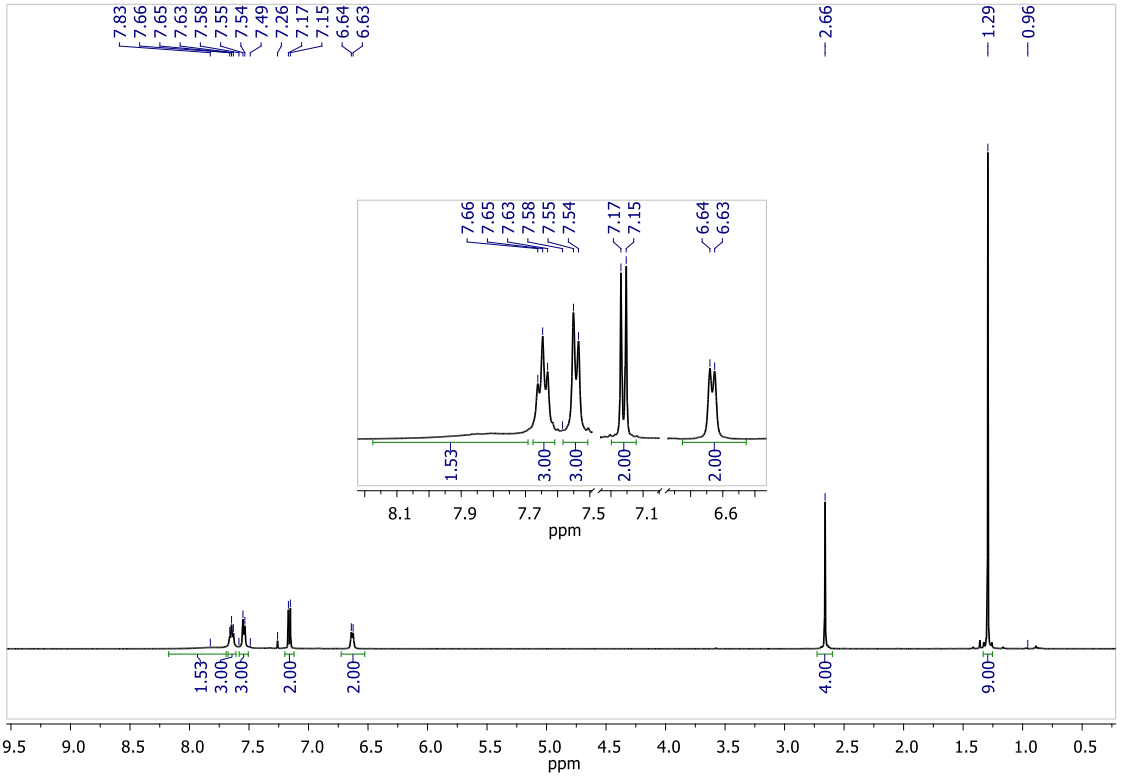

Figure S29. ^{1}H NMR spectrum of **[*t*-BuPhB{2-(6-(CF$_3$)Py)}$_3$]Au(C$_2$H$_4$)** in $CDCl_3$

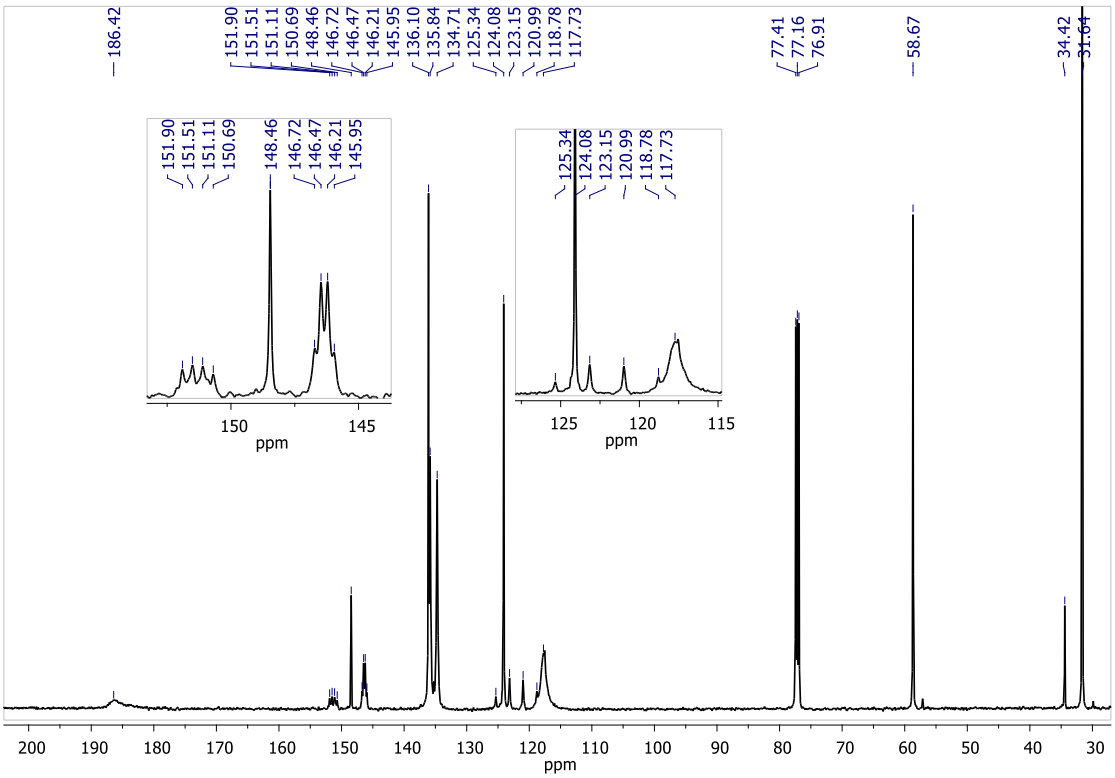

Figure S30. ^{13}C NMR spectrum of **[*t*-BuPhB{2-(6-(CF$_3$)Py)}$_3$]Au(C$_2$H$_4$)** in $CDCl_3$

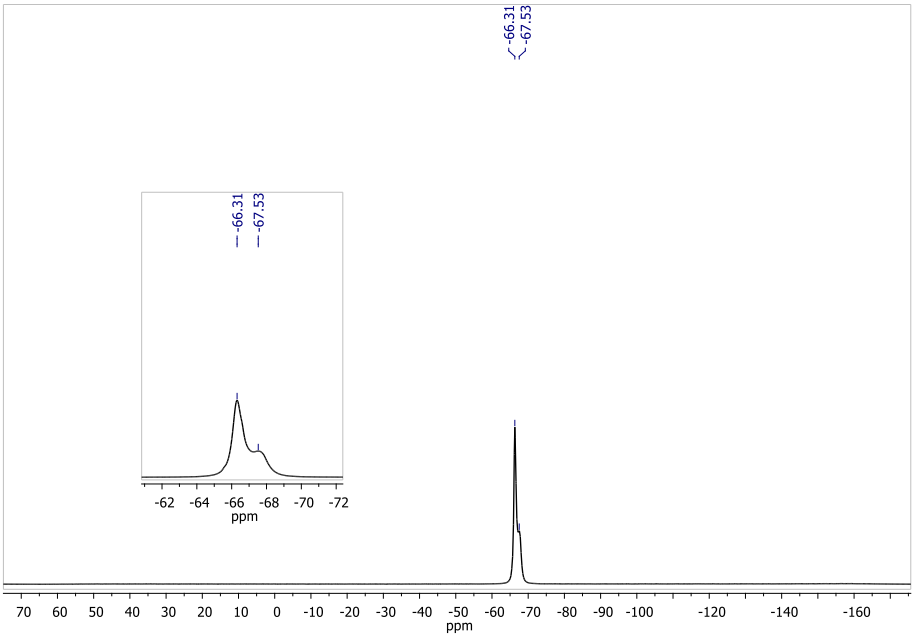

Figure S31 ^{19}F NMR spectrum of **[*t*-BuPhB{2-(6-(CF$_3$)Py)}$_3$]Au(C$_2$H$_4$)** in $CDCl_3$

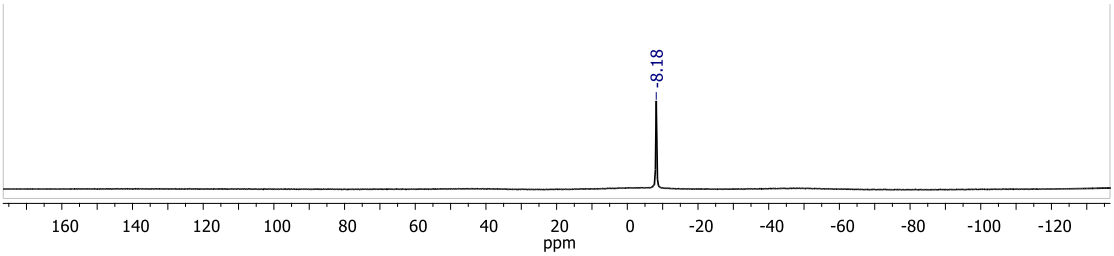

Figure S32. ^{11}B NMR spectrum of **[*t*-BuPhB{2-(6-(CF$_3$)Py)}$_3$]Au(C$_2$H$_4$)** in $CDCl_3$

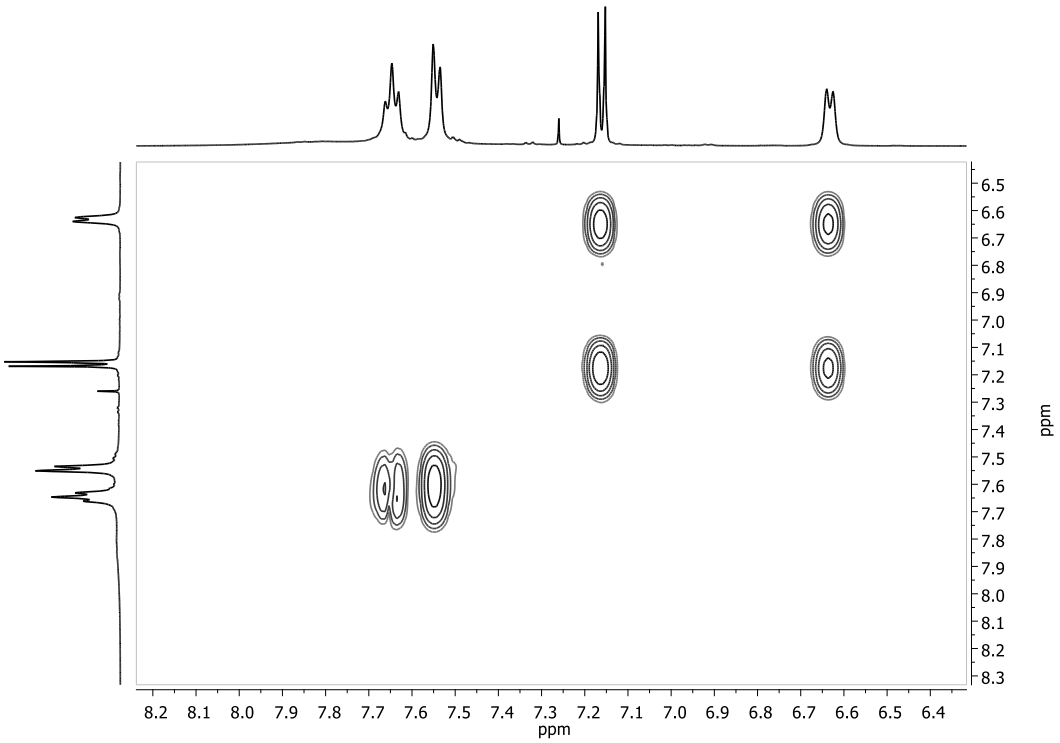

Figure S33. COSY spectrum of **[*t*-BuPhB{2-(6-(CF$_3$)Py)}$_3$]Au(C$_2$H$_4$)** in $CDCl_3$

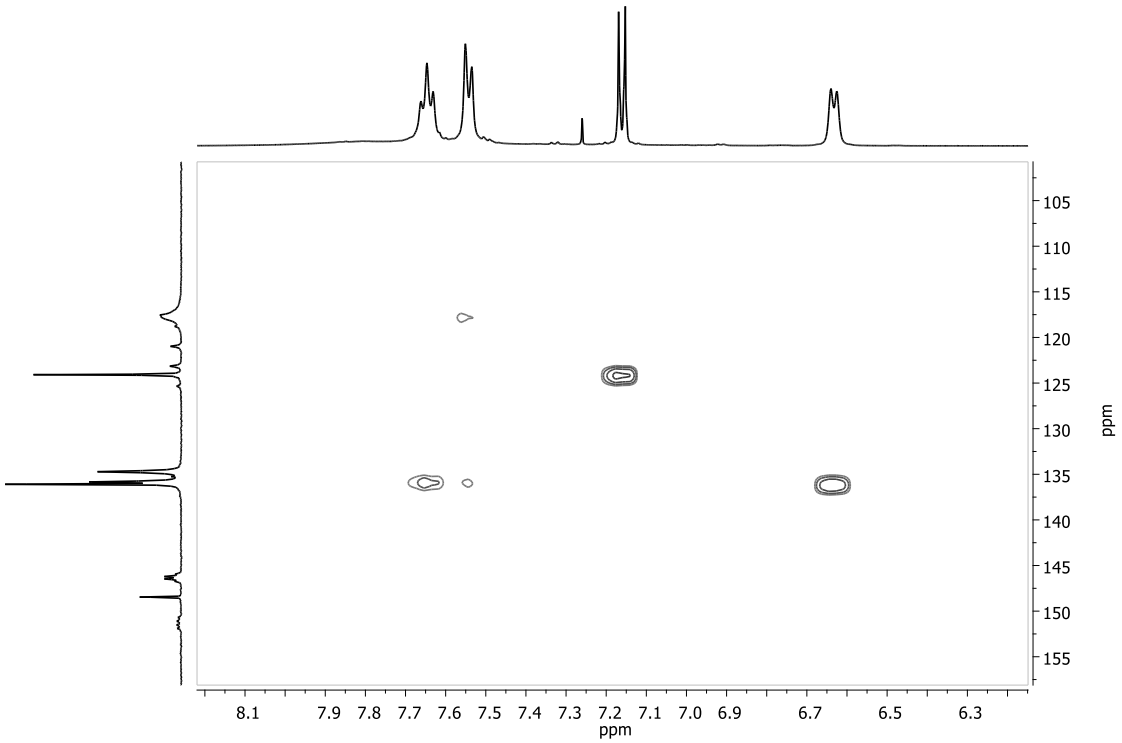

Figure S34. HSQC spectrum of **[*t*-BuPhB{2-(6-(CF$_3$)Py)}$_3$]Au(C$_2$H$_4$)** in $CDCl_3$

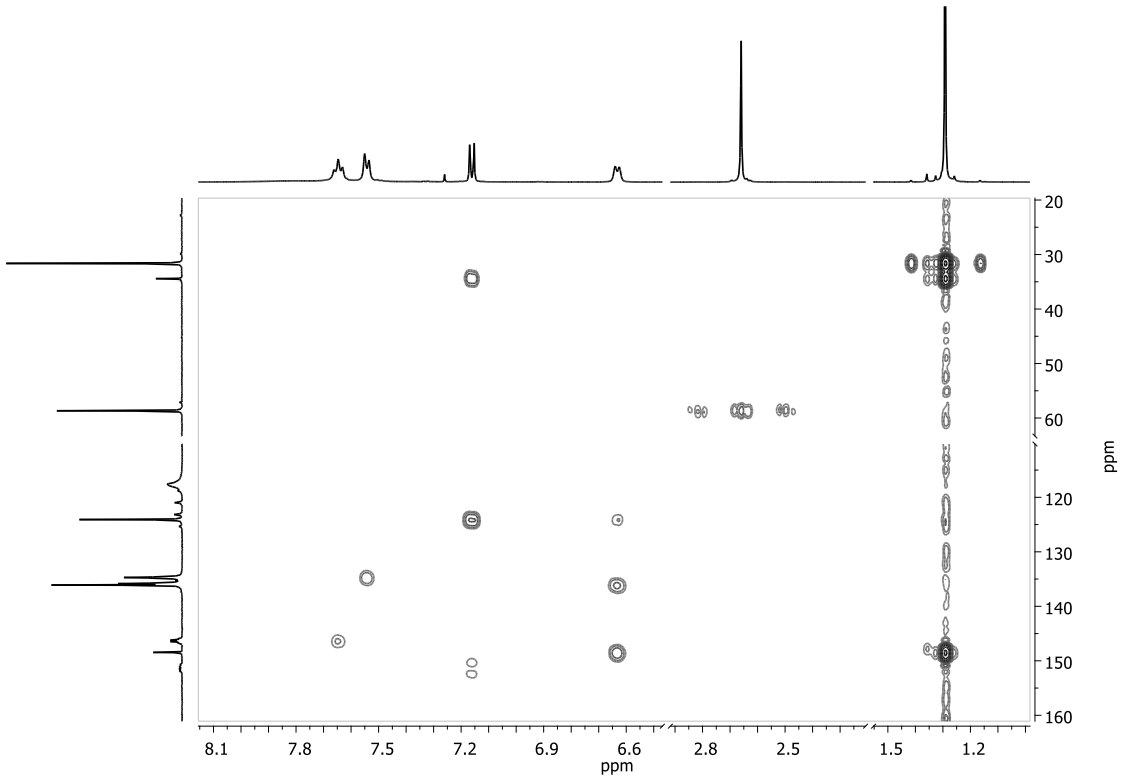

Figure S35. HMBC spectrum of **[*t*-BuPhB{2-(6-(CF$_3$)Py)}$_3$]Au(C$_2$H$_4$)** in $CDCl_3$

Table S1. Selected bond distances (Å), angles (°), and NMR spectroscopic data (ppm) of TpybM(C_2H_4) (Tpyb^{CF3} = [*t*-BuPhB(6-(CF_3)Py)$_3$]; M = Cu, Ag, Au). The M•••C(B) ipso-carbon separation between the M and flanking aryl group, and M••B separation in italics. ∑ at M represents the sum of angles at M involving two nitrogen atoms bonded to M and the centroid of the C=C. Data on tris(pyrazolyl)borate analog Tp^{CF3}Ag(C_2H_4) and Tp^{C2F5}M(C_2H_4) are also included (Tp^{CF3} = [PhB(3-(CF_3)Pz)$_3$], Tp^{C2F5} = [PhB(3-(C_2F_5)Pz)$_3$]) for comparisons.

Molecule	**Tpyb**^{CF3}Cu(C_2H_4)	**Tpyb**^{CF3}Ag(C_2H_4)	**Tpyb**^{CF3}Au(C_2H_4)	**Tp**^{CF3}Ag(C_2H_4)	**Tp**^{C2F5}Cu(C_2H_4)	**Tp**^{C2F5}Ag(C_2H_4)	**Tp**^{C2F5}Au(C_2H_4)
C=C	1.346(6)	1.338(4)	1.399(4)	1.296(7)	1.354(7)	1.311(5)	1.366(12)
M-C	2.046(3), 2.036(3)	2.294(2), 2.292(2)	2.108(2), 2.104(2)	2.262(4), 2.267(4)	2.027(4), 2.033(4)	2.279(3), 2.286(3)	2.089(8), 2.105(7)
M-N	2.032(2), 2.037(2)	2.2930(18), 2.3184(17)	2.2280(19), 2.2185(19)	2.273(3), 2.248(3)	2.008(3), 2.009(3)	2.279(2), 2.286(2)	2.213(6), 2.216(6)
M••C(B)	*2.601(3)*	*2.5740(18)*	*2.760(2)*	*2.868(3)*			
M••B	*2.866(3)*	*3.047(2)*	*3.092(2)*	*3.157(4)*	*2.949*	*3.129*	*3.231*
C-M-C	38.49(17)	33.93(10)	38.80(11)	33.25(18)	38.96(19)	33.38(14)	38.0(3)
N-M-N	92.33(9)	85.91(6)	83.07(7)	84.23(9)	93.76(13)	86.02(7)	84.7(2)
∑ at M	359.9	359.1	360.0	359.9	360	360	360
^{1}H *H_2*C=	3.57	4.66	2.66	4.72	3.71	4.62	2.85
^{13}C H$_2$*C*=	85.13	103.15	58.67	101.7	85.5	101.6	58.9
reference	This work	This work	This work	[3]	[4]	[4]	[4]

X-ray Structure Determinations. A suitable crystal covered with a layer of hydrocarbon/Paratone-N oil was selected and mounted on a Cryo-loop, and immediately placed in the low temperature nitrogen stream. The X-ray intensity data were collected on a Bruker D8 Quest equipped with a PHOTON II 7 CPAD detector and an Oxford Cryosystems 700 series cooler, a Triumph graphite monochromator, and a Mo Kα fine-focus sealed tube (λ = 0.71073 Å). The data of the [*t*-BuPhB(6-$(CF_3)Py)_3$]Cu(C_2H_4) were collected at a higher temperature of 190(2) K (because crystals tend to crack at 100 K) while those of the related Ag and Au complexes and [*t*-BuPhB(6-$(CF_3)Py)_3$]H were measured at 100(2) K. Intensity data were processed using the Bruker Apex4 program suite. Absorption corrections were applied by using SADABS.[5] Initial atomic positions were located by SHELXT,[6] and the structures of the compounds were refined by the least-squares method using SHELXL[7] within Olex2 GUI.[8] All the non-hydrogen atoms were refined anisotropically. All the hydrogen atoms (except those on ethylene of the Ag and Au complexes, and on nitrogen of the free ligand) were included at calculated positions and refined using appropriate riding models. The hydrogen atoms on ethylene carbons of the Ag and Au complexes and on nitrogen of [*t*-BuPhB(6-$(CF_3)Py)_3$]H were located in the difference map and refined freely.

CheckCif indicated C-level, ADDSYM alerts for [*t*-BuPhB(6-$(CF_3)Py)_3$]Cu(C_2H_4) and [*t*-BuPhB(6-$(CF_3)Py)_3$]Au(C_2H_4) complexes. However, more detailed analysis using Platon ADDSYM run did not reveal an alternative option apart from $P2_1/n$. As an additional test, we solved and refined the structure of [*t*-BuPhB(6-$(CF_3)Py)_3$]Au(C_2H_4) also in $P2_1/m$ in a smaller unit cell (a = 11.6597 Å, b = 10.3872 Å, c = 12.7188 Å, β = 109.706°, V = 1450.18 Å^3). However, except for the Au-C_2H_4 fragment, refinement in this space group required the use of significant whole molecule disorder model over a mirror plane. The room temperature data of the same sample was also collected and found to be a clear fit for $P2_1/m$ (a = 11.6718(10) Å, b = 10.5613(9) Å, c = 12.8825(10) Å, β = 107.638(4)°, V = 1513.4(2) Å^3, Z = 2), and refined well with minor (acceptable) disorder. Overall, $P2_1/n$ is the better, correct option at 100K for [*t*-BuPhB(6-$(CF_3)Py)_3$]Au(C_2H_4). X-ray structural figures were generated using Olex2.

CCDC files with numbers 2126166-2126168 contain the supplementary crystallographic data for [*t*-BuPhB(6-$(CF_3)Py)_3$]M(C_2H_4) (M = Cu, Ag, Au), while 2126169 and 2126170

represent 100K data on [*t*-BuPhB(6-(CF_3)Py)$_3$]H and room temperature data on [*t*-BuPhB(6-(CF_3)Py)$_3$]Au(C_2H_4). These data can be obtained free of charge via http://www.ccdc.cam.ac.uk/conts/retrieving.html or from the Cambridge Crystallographic Data Centre (CCDC), 12 Union Road, Cambridge, CB2 1EZ, UK). Additional details are provided in supporting information section.

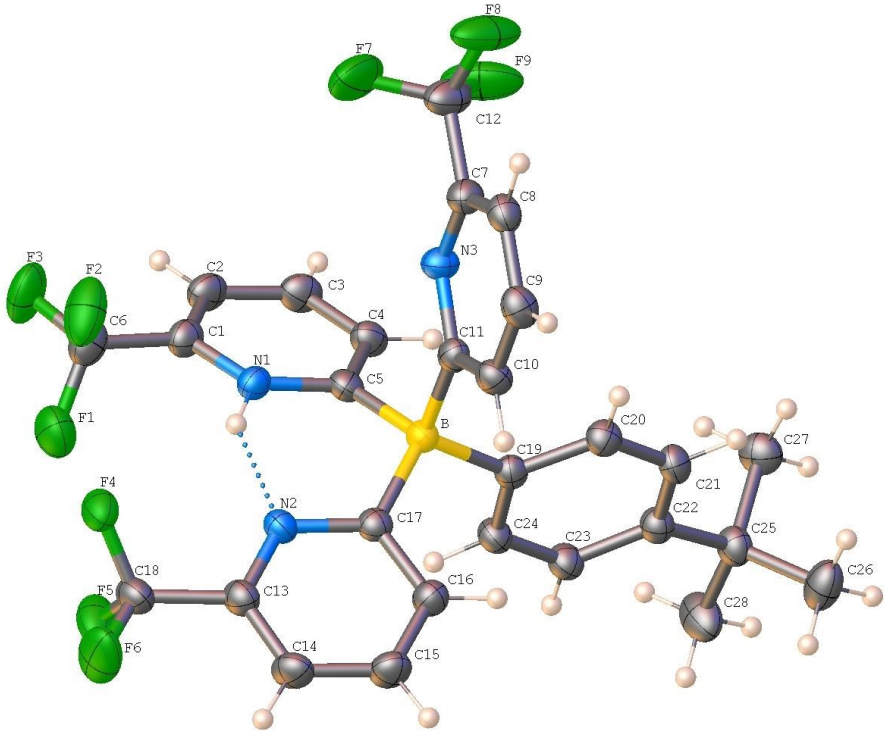

Figure S36. A view of [*t*-BuPhB(6-(CF_3)Py)$_3$]H and the atom numbering scheme

Table S2. Crystal data and structure refinement for [*t*-BuPhB(6-(CF_3)Py)$_3$]H.

Identification code	HRD50
Empirical formula	$C_{28}H_{23}BF_9N_3$
Formula weight	583.30
Temperature/K	100.00
Crystal system	monoclinic
Space group	$P2_1/n$
a/Å	10.4400(6)
b/Å	20.0684(12)
c/Å	13.0151(8)

α/°	90
β/°	101.246(2)
γ/°	90
Volume/Å^3	2674.5(3)
Z	4
ρ_{calc}g/cm^3	1.449
μ/mm^{-1}	0.129
F(000)	1192.0
Crystal size/mm^3	0.22 × 0.2 × 0.08
Radiation	Mo Kα (λ = 0.71073)
2Θ range for data collection/°	5.018 to 55.75
Index ranges	-13 ≤ h ≤ 13, -26 ≤ k ≤ 26, -17 ≤ l ≤ 17
Reflections collected	69590
Independent reflections	6376 [R_{int} = 0.0457, R_{sigma} = 0.0288]
Data/restraints/parameters	6376/0/378
Goodness-of-fit on F^2	1.167
Final R indexes [I>=2σ (I)]	R_1 = 0.0707, wR_2 = 0.1817
Final R indexes [all data]	R_1 = 0.1169, wR_2 = 0.2480
Largest diff. peak/hole / e Å^{-3}	0.48/-0.51

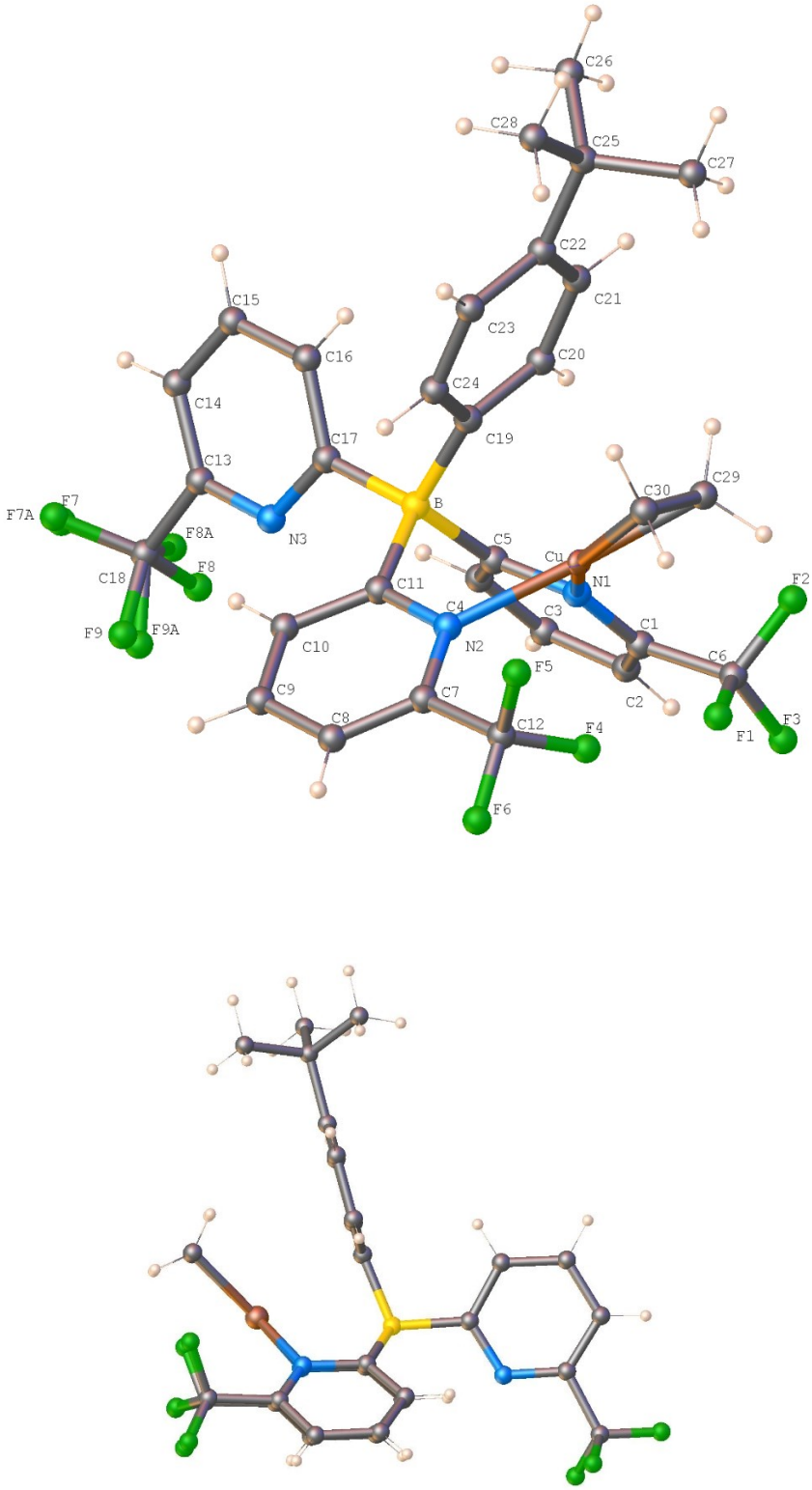

Figure S37. Two views of [*t*-BuPhB(6-(CF_3)Py)$_3$]Cu(C_2H_4) and the atom numbering scheme

Table S3. Crystal data and structure refinement for [*t*-BuPhB(6-(CF_3)Py)$_3$]Cu(C_2H_4).

Identification code	HRD57
Empirical formula	$C_{30}H_{26}BCuF_9N_3$
Formula weight	673.89
Temperature/K	190.00
Crystal system	monoclinic
Space group	$P2_1/n$
a/Å	11.6525(6)
b/Å	10.4312(6)
c/Å	24.2415(12)
α/°	90
β/°	98.454(3)
γ/°	90
Volume/Å^3	2914.5(3)
Z	4
ρ_{calc}g/cm^3	1.536
μ/mm^{-1}	0.833
F(000)	1368.0
Crystal size/mm^3	0.28 × 0.2 × 0.18
Radiation	Mo Kα (λ = 0.71073)
2Θ range for data collection/°	5.268 to 58.336
Index ranges	$-15 \leq h \leq 15$, $-14 \leq k \leq 14$, $-33 \leq l \leq 33$
Reflections collected	39559
Independent reflections	7851 [R_{int} = 0.0357, R_{sigma} = 0.0271]
Data/restraints/parameters	7851/48/428
Goodness-of-fit on F^2	1.072
Final R indexes [I>=2σ (I)]	R_1 = 0.0586, wR_2 = 0.1268
Final R indexes [all data]	R_1 = 0.0764, wR_2 = 0.1345
Largest diff. peak/hole / e Å^{-3}	0.48/-0.33

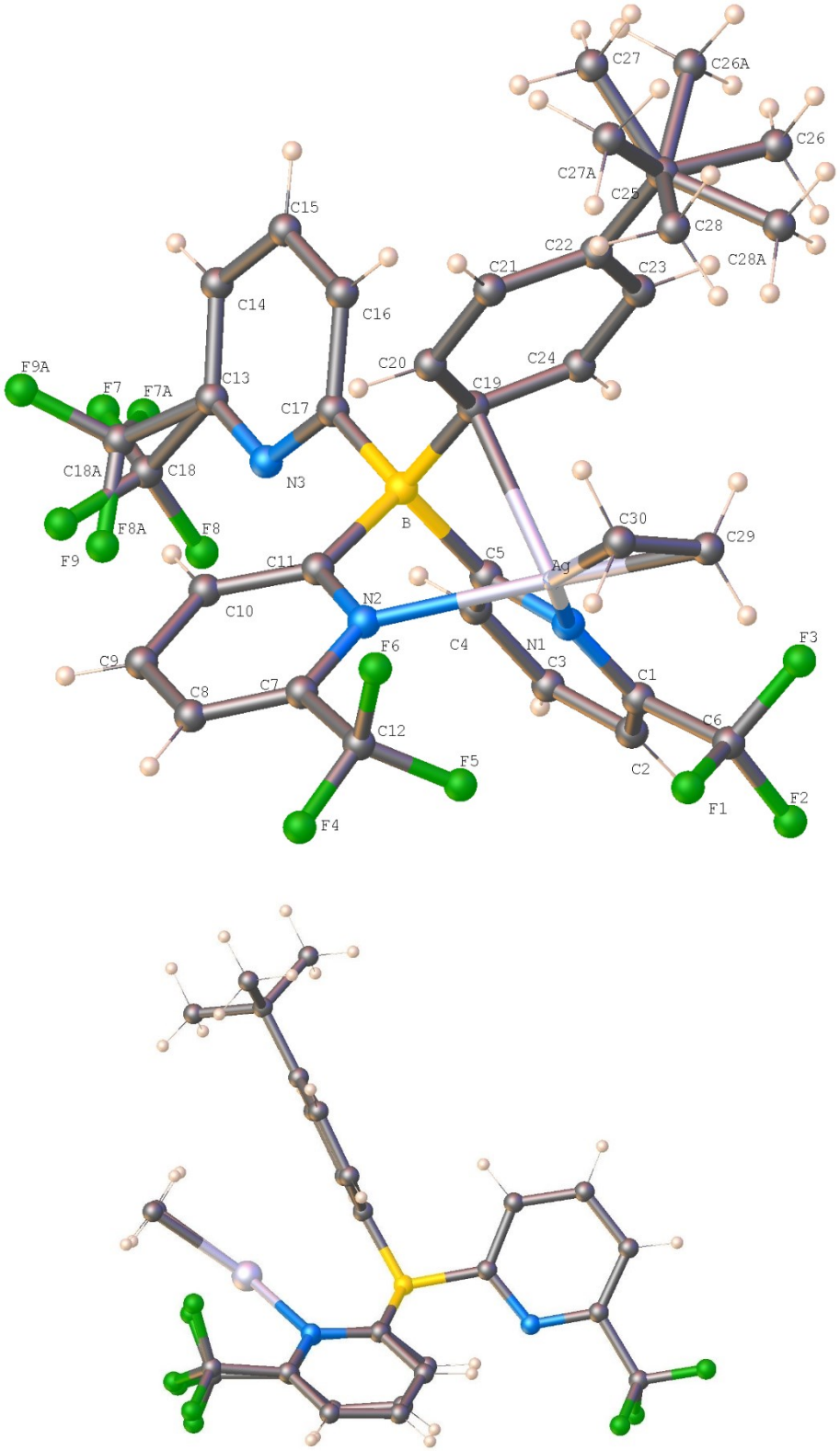

Figure S38. Two views of [*t*-BuPhB(6-(CF_3)Py)$_3$]Ag(C_2H_4) and the atom numbering scheme

Table S4. Crystal data and structure refinement for [*t*-BuPhB(6-(CF_3)Py)$_3$]Ag(C_2H_4).

Identification code	HRD53
Empirical formula	$C_{30}H_{26}AgBF_9N_3$
Formula weight	718.22
Temperature/K	100.00
Crystal system	triclinic
Space group	P-1
a/Å	10.2339(4)
b/Å	12.0369(4)
c/Å	12.9756(4)
α/°	72.0740(10)
β/°	89.2980(10)
γ/°	73.7390(10)
Volume/Å^3	1455.17(9)
Z	2
ρ_{calc}g/cm^3	1.639
μ/mm^{-1}	0.777
F(000)	720.0
Crystal size/mm^3	0.25 × 0.2 × 0.18
Radiation	Mo Kα (λ = 0.71073)
2Θ range for data collection/°	5.102 to 66.282
Index ranges	$-15 \leq h \leq 15$, $-18 \leq k \leq 18$, $-19 \leq l \leq 19$
Reflections collected	27189
Independent reflections	10786 [R_{int} = 0.0214, R_{sigma} = 0.0287]
Data/restraints/parameters	10786/55/484
Goodness-of-fit on F^2	1.026
Final R indexes [I>=2σ (I)]	R_1 = 0.0398, wR_2 = 0.0820
Final R indexes [all data]	R_1 = 0.0462, wR_2 = 0.0859
Largest diff. peak/hole / e Å^{-3}	1.28/-1.01

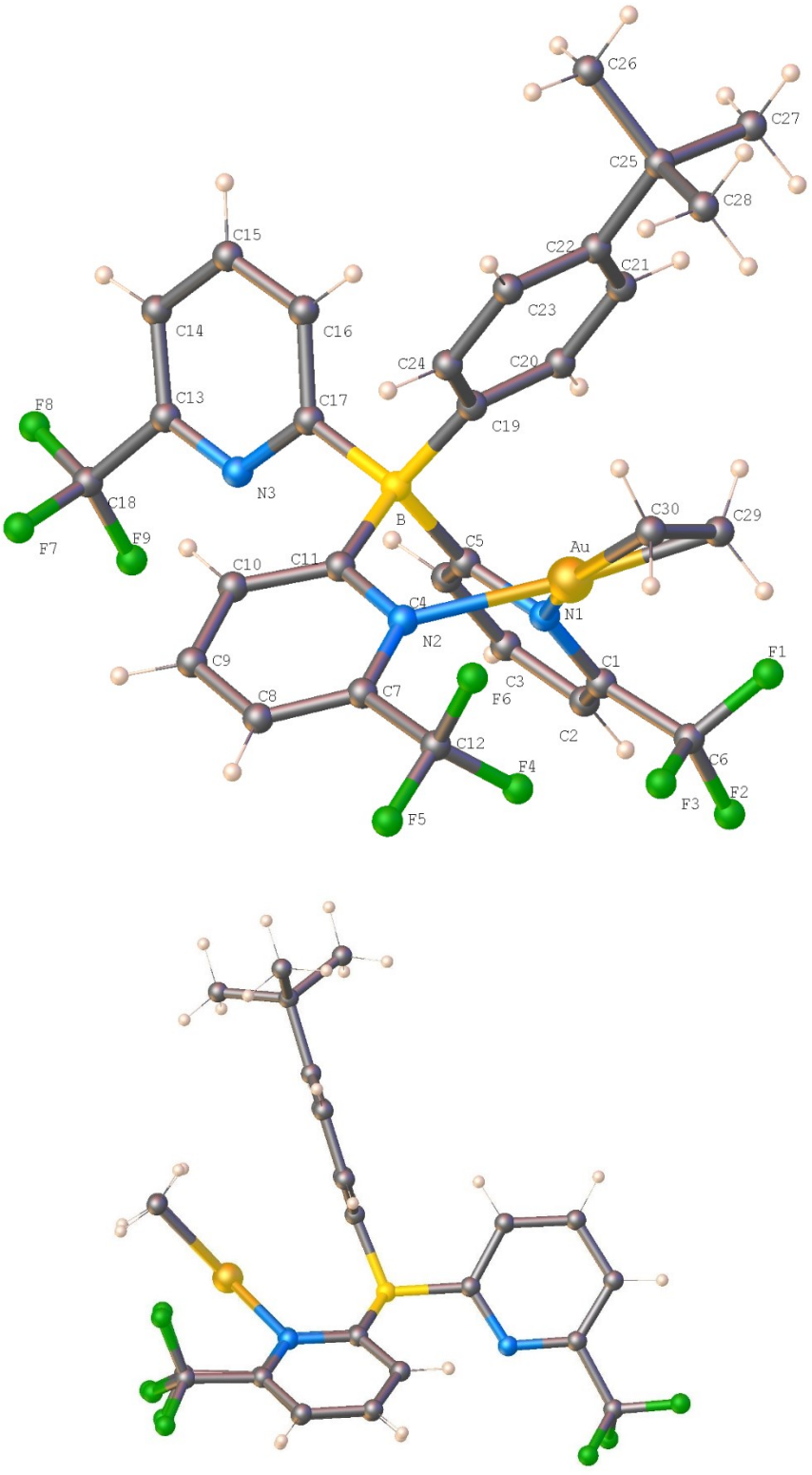

Figure S39. Two views of [*t*-BuPhB(6-(CF_3)Py)$_3$]Au(C_2H_4) and the atom numbering scheme

Table S5. Crystal data and structure refinement for [*t*-BuPhB(6-(CF_3)Py)$_3$]Au(C_2H_4).

Identification code	HRD55
Empirical formula	$C_{30}H_{26}AuBF_9N_3$
Formula weight	807.31
Temperature/K	100.00
Crystal system	monoclinic
Space group	$P2_1/n$
a/Å	11.6594(4)
b/Å	10.3878(4)
c/Å	24.1447(8)
α/°	90
β/°	97.334(2)
γ/°	90
Volume/Å^3	2900.37(18)
Z	4
ρ_{calc}g/cm^3	1.849
μ/mm^{-1}	5.157
F(000)	1568.0
Crystal size/mm^3	0.18 × 0.16 × 0.06
Radiation	Mo Kα (λ = 0.71073)
2Θ range for data collection/°	5.676 to 66.28
Index ranges	$-17 \leq h \leq 17$, $-15 \leq k \leq 15$, $-36 \leq l \leq 37$
Reflections collected	53841
Independent reflections	11004 [R_{int} = 0.0248, R_{sigma} = 0.0189]
Data/restraints/parameters	11004/0/417
Goodness-of-fit on F^2	1.012
Final R indexes [I>=2σ (I)]	R_1 = 0.0226, wR_2 = 0.0414
Final R indexes [all data]	R_1 = 0.0382, wR_2 = 0.0485
Largest diff. peak/hole / e Å^{-3}	1.81/-1.63

Computational Details

Density Functional Theory calculations were carried out by using relativistic methods employing the ADF code[9] with the all-electron triple-ζ Slater basis set plus the double-polarization (STO-TZ2P) basis set in conjunction with the Becke-Perdew (BP86) functional[10] via the generalized gradient approximation (GGA). London dispersion corrections were taken into account via the pairwise Grimme (BP86-D3) approach.[11]Geometry optimizations were performed via the analytical energy gradient method implemented by Versluis and Ziegler,[12] with energy convergence criteria set at 10^{-4} Hartree, gradient convergence criteria at 10^{-4} Hartree/Å, and radial convergence of 10^{-3} Å, without any symmetry restrain. Scalar relativistic effects were considered through the ZORA Hamiltonian.[13]

The interaction energy is further dissected into several chemically meaningful terms according to the Energy Decomposition Analysis (EDA) of Ziegler and Rauk,[14, 15]

$$\Delta E_{int} = \Delta E_{Pauli} + \Delta E_{elstat} + \Delta E_{orb} + \Delta E_{disp}$$

where ΔE_{Pauli} term involves the electron repulsion between occupied orbitals from the different fragments. ΔE_{elstat} and ΔE_{orb} are related to the stabilizing electrostatic and covalent character of the interaction, respectively. The contribution from dispersion interaction (ΔE_{disp}) is evaluated using the pairwise correction of Grimme (D3). Bonding analysis is given in terms of bonding contributions to ΔE_{orb} by using the Natural Orbitals for Chemical Valence extension of the EDA method (EDA-NOCV),[16] resulting in deformation densities accounting for the individual in- and out-flow of charges related to the bonding pattern.

Table S6. Energy decomposition analyses for the C_2H_4-M interaction, for [*t*-BuPhB(6-$(CF_3)Py)_3]^-$, [PhB(6-$(CF_3)Py)_3]^-$, [PhB(6-$(CF_3)Pz)_3]^-$, and [*t*-BuPhB(6-$(CF_3)Pz)_3]^-$ ligand complexes, in two coordination modes, namely, κ^2- and κ^3-. Values in kcal·mol^{-1}. In addition the contribution from both π_2^*-backbonding and σ-donation is given accounting for π_2*-C_2H_4 ← M and π_1-C_2H_4 → M bonding schemes, respectively.

	κ^2-Cu		κ^2-Ag		κ^2-Au		κ^3-Cu		κ^3-Ag		κ^3-Au	
[*t*-BuPhB(6-$(CF_3)Py)_3]^-$												
ΔE_{Pauli}	115.7		93.9		211.7		114.0		71.2		201.5	
ΔE_{Elstat}	-92.1	57.6%	-75.7	61.8%	-165.8	60.4%	-87.8	58.9%	-56.5	61.2%	-153.7	61.0%
ΔE_{Orb}	-54.6	34.2%	-37.7	30.8%	-98.6	36.0%	-49.4	33.1%	-27.9	30.2%	-89.3	35.4%
ΔE_{Disp}	-13.1	8.2%	-9.2	7.5%	-9.9	3.6%	-11.8	7.9%	-7.9	8.6%	-9.0	3.6%
ΔE_{int}	-44.1		-28.7		-62.7		-35.0		-21.1		-50.4	
π_2*-C_2H_4←M	-28.9	52.9%	-17.5	46.3%	-49.0	49.6%	-23.3	47.1%	-10.2	36.5%	-40.1	44.9%
π_1-C_2H_4→M	-17.0	31.1%	-12.9	34.2%	-35.7	36.2%	-16.9	34.2%	-11.6	41.6%	-35.6	39.9%
[PhB(6-$(CF_3)Py)_3]^-$	κ^2-Cu		κ^2-Ag		κ^2-Au		κ^3-Cu		κ^3-Ag		κ^3-Au	
ΔE_{Pauli}	114.5		110.5		207.0		115.4		69.2		108.4	
ΔE_{Elstat}	-91.6	58.0%	-89.0	64.3%	-162.7	60.7%	-85.3	58.8%	-54.1	60.8%	-79.0	58.5%
ΔE_{Orb}	-54.5	34.5%	-42.3	30.6%	-97.0	36.2%	-47.9	33.1%	-26.4	29.7%	-44.3	32.8%
ΔE_{Disp}	-11.9	7.5%	-7.1	5.1%	-8.2	3.1%	-11.8	8.2%	-8.4	9.4%	-11.7	8.6%
ΔE_{int}	-43.5		-27.9		-61.0		-29.6		-19.6		-26.6	
π_2*-C_2H_4←M	-28.9	53.0%	-22.9	54.1%	-47.8	49.3%	-22.6	47.2%	-9.5	36.1%	-19.8	44.6%
π_1-C_2H_4→M	-17.0	31.1%	-13.9	32.8%	-35.9	37.0%	-16.5	34.3%	-11.1	41.8%	-15.8	35.6%

[PhB(3-(CF$_3$)Pz)$_3$]$^-$	κ^2-Cu		κ^2-Ag		κ^2-Au		κ^3-Cu		κ^3-Ag		κ^3-Au	
ΔE_{Pauli}	113.5		101.3		199.4		110.7		86.6		194.3	
ΔE_{Elstat}	-94.0	58.7%	-84.1	64.2%	-161.5	61.1%	-89.9	59.0%	-72.3	63.7%	-156.4	61.4%
ΔE_{Orb}	-56.4	35.2%	-41.9	32.0%	-97.2	36.8%	-52.0	34.1%	-35.6	31.4%	-91.8	36.0%
ΔE_{Disp}	-9.6	6.0%	-4.9	3.7%	-5.8	2.2%	-10.5	6.9%	-5.7	5.0%	-6.7	2.6%
ΔE_{int}	-46.6		-29.6		-65.0		-41.6		-26.9		-60.5	
π_2*-C_2H_4←M	-31.8	56.4%	-21.0	50.1%	-49.7	51.1%	-28.1	54.0%	-16.4	46.2%	-45.1	49.1%
π_1-C_2H_4→M	-16.6	29.4%	-13.7	32.6%	-35.1	36.1%	-16.0	30.7%	-12.7	35.8%	-34.3	37.4%
[*t*-BuPhB(3-(CF$_3$)Pz)$_3$]$^-$	κ^2-Cu		κ^2-Ag		κ^2-Au		κ^3-Cu		κ^3-Ag		κ^3-Au	
ΔE_{Pauli}	114.2		100.8		199.5		111.7		94.1		110.8	
ΔE_{Elstat}	-94.1	58.4%	-83.3	63.2%	-161.5	60.6%	-90.4	59.1%	-77.8	63.9%	-89.8	59.0%
ΔE_{Orb}	-56.3	34.9%	-41.7	31.7%	-97.8	36.7%	-52.2	34.1%	-38.1	31.3%	-51.8	34.1%
ΔE_{Disp}	-10.9	6.8%	-6.7	5.1%	-7.1	2.7%	-10.5	6.9%	-5.8	4.7%	-10.5	6.9%
ΔE_{int}	-47.1		-30.9		-66.9		-41.4		-27.6		-41.3	
π_2*-C_2H_4←M	-31.5	56.0%	-20.6	49.4%	-50.4	51.6%	-28.3	54.2%	-18.9	49.7%	-28.0	54.0%
π_1-C_2H_4→M	-16.4	29.1%	-13.5	32.3%	-34.7	35.4%	-15.9	30.5%	-12.6	33.1%	-15.8	30.6%

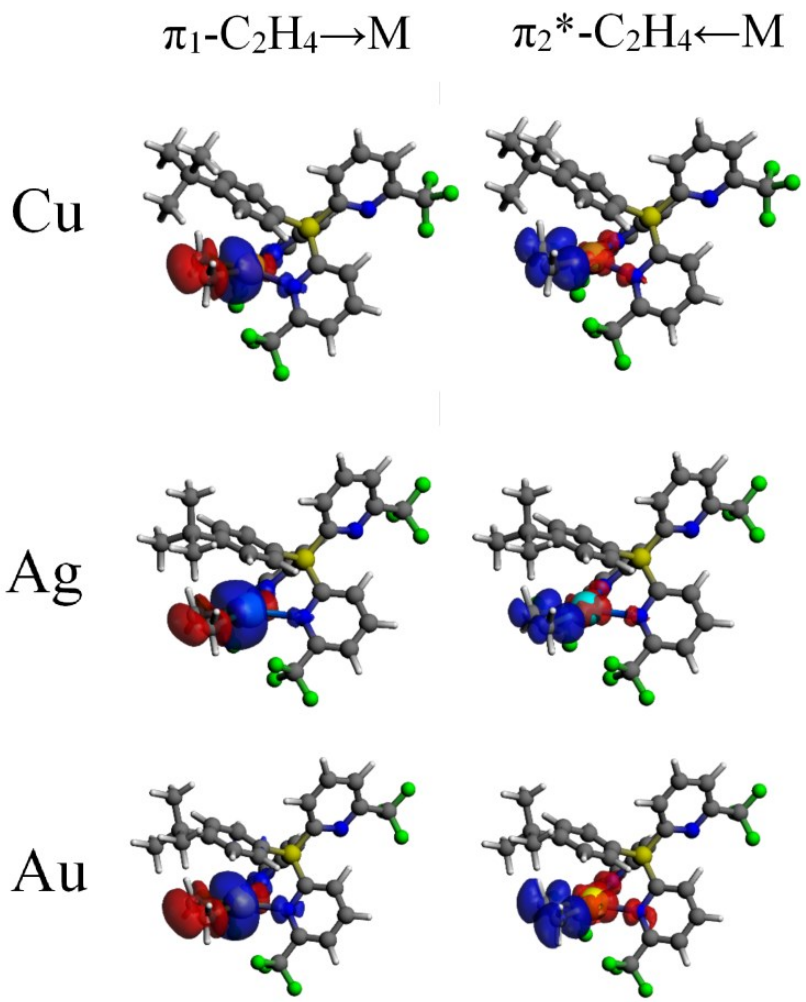

Figure S40: Selected deformation densities from the NOCV-EDA analysis, for κ^2-[*t*-BuPh$_2$B(6-(CF$_3$)Py)$_3$]M(C$_2$H$_4$), accounting for σ-donation (left) and π-backbonding (right). Charge flow from red to blue.

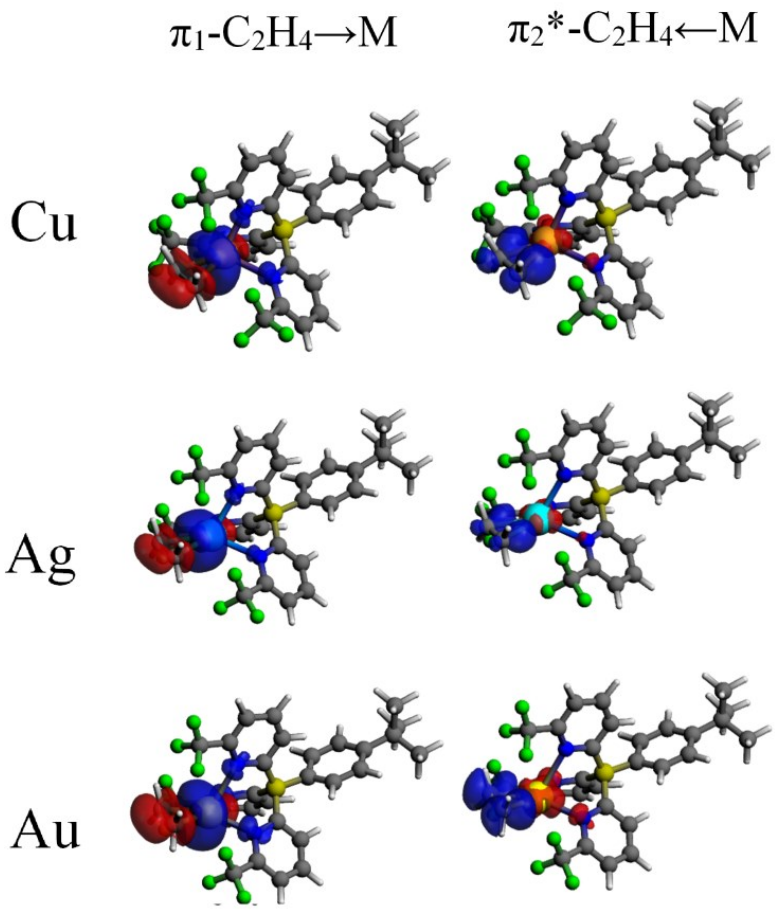

Figure S41: Selected deformation densities from the NOCV-EDA analysis, for κ^3-[*t*-BuPh$_2$B(6-(CF$_3$)Py)$_3$]M(C$_2$H$_4$), accounting for σ-donation (left) and π-backbonding (right). Charge flow from red to blue.

Table S7. Energy difference between the molecules of two different coordination modes, namely, κ^2- and κ^3- for [*t*-BuPhB(6-(CF_3)Py)$_3$]M(C_2H_4), [PhB(6-(CF_3)Py)$_3$]M(C_2H_4), [PhB(6-(CF_3)Pz)$_3$]M(C_2H_4), and [*t*-BuPhB(6-(CF_3)Pz)$_3$]M(C_2H_4) complexes (M = Cu, Ag, Au). Values in kcal·mol^{-1}. In all cases the κ^2-coordination mode is favored.

M =	Cu	Ag	Au
[*t*-BuPhB(6-(CF_3)Py)$_3$]M(C_2H_4)	13.7	13.6	21.5
[PhB(6-(CF_3)Py)$_3$]M(C_2H_4)	19.7	12.6	24.9
[PhB(3-(CF_3)Pz)$_3$]M(C_2H_4)	5.6	5.6	8.2
[*t*-BuPhB(3-(CF_3)Pz)$_3$]M(C_2H_4)	5.5	5.2	10.9

References:

1. Y. Qin, I. Kiburu, S. Shah and F. Jäkle, *Org. Lett.*, 2006, **8**, 5227-5230.
2. M. Ohashi, T. Adachi, N. Ishida, K. Kikushima and S. Ogoshi, *Angew. Chem., Int. Ed.*, 2017, **56**, 11911-11915.
3. H. V. R. Dias, J. Wu, X. Wang and K. Rangan, *Inorg. Chem.*, 2007, **46**, 1960-1962.
4. H. V. R. Dias and J. Wu, *Organometallics*, 2012, **31**, 1511-1517.
5. L. Krause, R. Herbst-Irmer, G. M. Sheldrick and D. Stalke, *J. Appl. Crystallogr.*, 2015, **48**, 3-10.
6. G. Sheldrick, *Acta Crystallogr. Sect. A: Found. Adv.*, 2015, **71**, 3-8.
7. G. Sheldrick, *Acta Crystallogr. Sect. C: Struct. Chem.*, 2015, **71**, 3-8.
8. O. V. Dolomanov, L. J. Bourhis, R. J. Gildea, J. A. K. Howard and H. Puschmann, *J. Appl. Crystallogr.*, 2009, **42**, 339-341.
9. S. ADF 2019, Theoretical Chemistry, Vrije Universiteit, Amsterdam, The Netherlands, http://www.scm.com).
10. A. D. Becke, *Physical Review A*, 1988, **38**, 3098-3100.
11. S. Grimme, *WIREs Computational Molecular Science*, 2011, **1**, 211-228.
12. L. Versluis and T. Ziegler, *The Journal of Chemical Physics*, 1988, **88**, 322-328.
13. E. v. Lenthe, E. J. Baerends and J. G. Snijders, *The Journal of Chemical Physics*, 1994, **101**, 9783-9792.
14. M. v. Hopffgarten and G. Frenking, *WIREs Computational Molecular Science*, 2012, **2**, 43-62.
15. T. Ziegler and A. Rauk, *Theoretica chimica acta*, 1977, **46**, 1-10.
16. M. P. Mitoraj, A. Michalak and T. Ziegler, *Journal of Chemical Theory and Computation*, 2009, **5**, 962-975.